Photolysis of *cis*- and *trans*-$[Fe^{III}(cyclam)(N_3)_2]^+$ Complexes: Spectroscopic Characterization of a Nitridoiron(V) Species

Karsten Meyer, Eckhard Bill,* Bernd Mienert, Thomas Weyhermüller, and Karl Wieghardt*

Contribution from the Max-Planck-Institut für Strahlenchemie, Stiftstrasse 34-36, D-45470 Mülheim an der Ruhr, Germany

Received September 28, 1998. Revised Manuscript Received March 19, 1999

Abstract: Reaction of *cis*-$[Fe^{III}(cyclam)Cl_2]Cl$ in acidic H_2O/CH_3OH or CH_3CN/H_2O mixtures with NaN_3 at 50 °C produced upon addition of $NaClO_4$ or $NaPF_6$ the complex *trans*-$[Fe^{III}(cyclam)(N_3)_2]ClO_4$ (**1a**) or the hexafluorophosphate salt **1b**, whereas at −18 °C the same reaction produced *cis*-$[Fe^{III}(cyclam)(N_3)_2](ClO_4)$ (**2**) (cyclam = 1,4,8,11-tetraazacyclotetradecane). The crystal structures of **1b** and **2** were determined by single-crystal X-ray crystallography. Complexes **1a**, **b**, contain a low-spin ($S = {}^1/_2$) and **2**, a high-spin ferric ion ($S = {}^5/_2$) as was established by variable-temperature magnetic susceptibility measurements and Mössbauer and X-band EPR spectroscopy. The low-spin *trans*-$[(cyclam)Fe^{II}(N_3)_2]$ and high-spin *cis*-$[(cyclam)Fe^{II}(N_3)_2]$ species were generated electrochemically in CH_3CN solution and were characterized by Mössbauer spectroscopy. Photolysis of **1a** in CH_3CN at −35 °C and 20 °C with a Hg immersion lamp generated within 15 min a yellow solution. EPR and Mössbauer spectra show that a single high-valent species with an $S = {}^1/_2$ ground state is formed: $[\{trans\text{-}(cyclam)Fe(N_3)\}_2(\mu\text{-}N)]^{2+}$. The Mössbauer spectrum at 80 K exhibits two quadrupole doublets (ratio 1:1), indicating the presence of low-spin Fe^{IV} ($S = 1$) with isomer shift, δ, at 0.11 mm s^{-1} and quadrupole splitting, ΔE_Q, at 0.97 mm s^{-1} and *intermediate-spin* Fe^{III} ($S = {}^3/_2$) with $\delta = 0.20$ mm s^{-1} and $\Delta E_Q = 2.09$ mm s^{-1}. The valencies in this mixed valent $[Fe^{III}(\mu\text{-}N)Fe^{IV}]^{4+}$ core ($S_t = {}^1/_2$) are localized on the Mössbauer time scale. In addition 18% of a low-spin Fe^{II} complex ($S = 0$) was found with $\delta = 0.54$ mm s^{-1}, $\Delta E_Q = 0.65$ mm s^{-1}. Photolysis of **2** at −35 °C in CH_3CN produced a yellow mixed valent dinuclear species with an $S = {}^3/_2$ ground state. For this species we propose the structure $[\{cis\text{-}(cyclam)Fe^{III}(N_3)\}(\mu\text{-}N)\{trans\text{-}(cyclam)Fe^{IV}(N_3)\}]^{2+}$ with an $[Fe^{III}(\mu\text{-}N)Fe^{IV}]^{2+}$ core ($S_t = {}^3/_2$). The Mössbauer spectrum at 80 K clearly shows that the valencies are localized: two subspectra are detected (ratio 1:1) at (a) $\delta = 0.14$ mm s^{-1}, $\Delta E_Q = 0.81$ mm s^{-1} (Fe^{IV}; $S = 1$) and (b) $\delta = 0.50$ mm s^{-1}, $\Delta E_Q = 1.89$ mm s^{-1} (Fe^{III}; $S = {}^5/_2$). Strong intramolecular antiferromagnetic coupling between the two iron sites produces the observed $S_t = {}^3/_2$ ground state. The proposed spin states and spin-coupling schemes for both photolysis products were proven by magnetic Mössbauer and EPR spectra. The formation of the dinuclear species requires the primary formation of a nitridoiron(V) species: *trans*-$[N{=}Fe^{V}(cyclam)(N_3)]^+$. This intermediate has been detected during photolysis of frozen CH_3CN solutions of **1a** at 4 and 77 K by EPR and Mössbauer spectroscopy. The species contains an Fe^V ion (d^3, $S = {}^3/_2$) with an isomer shift $\delta = -0.04$ mm s^{-1} and a quadrupole splitting $\Delta E_Q = -1.90$ mm s^{-1} at 80 K. In addition, a five-coordinate ferrous species has been identified as a primary photolysis product which is formed via photolytic homolysis of the $Fe^{III}{-}N_3$ bond. Thus, simultaneous photo*oxidation* and -*reduction* processes occur during the photolysis of **1a** in frozen solution. The electronic structure of the Fe^V species was investigated with EPR, magnetic Mössbauer spectroscopy, and spin-Hamiltonian analyses.

Introduction

Dinuclear (μ-nitrido)diiron complexes with porphinato(2-)[1−6] or phthalocyaninato(2-)[7−12] ligands constitute an intensively studied class of compounds. They are fairly readily synthetically accessed from mononuclear azidoiron(III) species via thermolysis or photolysis. They have been shown to contain the linear mixed valent $[Fe^{3.5}(\mu\text{-}N)Fe^{3.5}]$ core with an $S_t = {}^1/_2$ ground state. Since the Mössbauer spectra of these species consist invariably—even at 4.2 K—of a single quadrupole doublet with isomer shifts, δ, ranging from 0.08 to 0.18 mm s^{-1}, it has been concluded that the excess electron is fully delocalized (class III according to Robin and Day[13]).

(1) Summerville, D. A.; Cohen, I. A. *J. Am. Chem. Soc.* **1976**, *98*, 1747.
(2) Buchler, J. W.; Dreher, C. *Z. Naturforsch., B: Anorg. Chem., Org. Chem.* **1984**, *39B*, 222.
(3) Scheidt, W. R.; Summerville, D. A.; Cohen, I. A. *J. Am. Chem. Soc.* **1976**, *98*, 6623.
(4) Bottomley, L. A.; Garrett, B. B. *Inorg. Chem.* **1982**, *21*, 1260.
(5) Schick, G. A.; Findsen, E. W.; Bocian, D. F. *Inorg. Chem.* **1982**, *21*, 2885.
(6) Kadish, K. M.; Bottomley, L. A.; Brace, J. G.; Winograd, N. *J. Am. Chem. Soc.* **1980**, *102*, 4341.
(7) Goedken, V. L.; Ercolani, C. *J. Chem. Soc., Chem. Commun.* **1984**, 378.
(8) Bottomley, L. A.; Gorce, J.-N.; Goedken, V. L.; Ercolani, C. *Inorg. Chem.* **1985**, *24*, 3733.
(9) Kennedy, B. J.; Murray, K. S.; Homburg, H.; Kalz, W. *Inorg. Chim. Acta* **1987**, *134*, 19.
(10) Ercolani, C.; Gardini, M.; Pennesi, G.; Rossi, G.; Russo, U. *Inorg. Chem.* **1988**, *27*, 422.
(11) Ercolani, C.; Hewage, S.; Heucher, R.; Rossi, G. *Inorg. Chem.* **1993**, *32*, 2975.
(12) Ercolani, C.; Jubb, J.; Pennesi, G.; Russo, U.; Trigiante, G. *Inorg. Chem.* **1995**, *34*, 2535.
(13) Robin, M. B.; Day, P. *Adv. Inorg. Chem. Radiochem.* **1967**, *10*, 247.

10.1021/ja983454t CCC: $18.00
Published on Web 05/11/1999

We have recently reported that photolysis of mononuclear *non-heme* azidoiron(III) complexes also generates (μ-nitrido)-diiron complexes containing the linear [Fe(μ-N)Fe]$^{4+}$ core[14,15] but with an $S_t = {}^3/_2$ ground state as in [{L(Cl$_4$-cat)Fe}$_2$(μ-N)] where L represents 1,4,7-trimethyl-1,4,7-triazacyclononane and Cl$_4$-cat is the tetrachlorocatecholate dianion. The Mössbauer spectrum revealed *two* quadrupole doublets of equal intensity. Mixed-valent species of this type were thus shown to belong to class I or II with localized valencies. The $S_t = {}^3/_2$ ground state results from an antiferromagnetically coupled high-spin ferric ($S = {}^5/_2$) and an Fe^{IV} ion ($S = 1$).

It has been recognized from the earliest studies by Summerville and Cohen[1] and by Buchler and Dreher[2] that the formation of the [Fe(μ-N)Fe]$^{4+}$ core from azidoiron(III) precursors most probably involves a very reactive nitridoiron(V) intermediate, which in solution could attack—in a bimolecular reaction—the precursor with formation of dinitrogen and a ferrous intermediate which would finally combine with [(tpp)Fe^{V}N], affording the mixed-valent dinuclear species [{(tpp)Fe$^{III/IV}$}$_2$(μ-N)] (eq 1−3). The ligand tpp represents the tetraphenylporphinate dianion.

$$[(\text{tpp})\text{Fe}^{III}(\text{N}_3)] \xrightarrow[\Delta H]{h\cdot\nu} [(\text{tpp})\text{Fe}^{V}{=}\text{N}] \qquad (1)$$

$$[(\text{tpp})\text{Fe}^{V}{=}\text{N}] + [(\text{tpp})\text{Fe}^{III}(\text{N}_3)] \rightarrow [\{(\text{tpp})\text{Fe}\}_2(\text{N}_4)] \rightarrow 2[(\text{tpp})\text{Fe}^{II}] + 2\text{N}_2 \qquad (2)$$

$$[(\text{tpp})\text{Fe}^{V}{=}\text{N}] + [(\text{tpp})\text{Fe}^{II}] \rightarrow [\{(\text{tpp})\text{Fe}^{3.5}\}_2(\mu\text{-N})] \qquad (3)$$

Although alternative routes and mechanisms have been discussed in the literature,[1] the first step involving nitridoiron(V) intermediates is common to all of these proposals.

In 1988 Nakamoto and Wagner have presented resonance Raman (RR) spectroscopic evidence[16,17] for the occurrence of [(tpp)Fe^{V}N] during laser photolysis of [(tpp)Fe^{III}(N$_3$)] in frozen solution at 30 K where the above bimolecular reaction steps yielding dinuclear species are effectively quenched. They have identified a ν(Fe=N) stretching frequency at 876 cm^{-1} which is at much lower frequency than in the corresponding stable complexes [(tpp)Cr^{V}≡N] (1017 cm^{-1})[18] or [(tpp)Mn^{V}≡N] (1047 cm^{-1}).[19] At that time it had not been possible to definitively establish the spin state of the putative [(tpp)Fe^{V}N] species ($S = {}^1/_2$ or ${}^3/_2$) but the low ν(Fe=N) frequency is suggestive of an $S = {}^3/_2$ spin state where two electrons occupy the two π-antibonding (with respect to the Fe=N bond) *e*-orbitals in a C_{4v} symmetric N=Fe^{V}N$_4$ core.[17] On the other hand, Sellmann and co-workers[20] have recently reported a five-coordinate, square-based pyramidal Fe^{V} species with an $S = {}^1/_2$ ground state.

In both of the above cases the tetradentate auxiliary ligands employed are, in principle, not redox (or spectroscopically) "innocent" in the sense that the electron distribution may not be correctly reflected by the assignment of a formal oxidation state +V to the metal ion which implies a d^3 electron configuration at the metal ion. It is conceivable that intramolecular anti- or ferromagnetic coupling between an Fe^{IV} (d^4 $S = 1$) and a radical ligand ($S = {}^1/_2$) produces the observed $S = {}^1/_2$ or ${}^3/_2$ ground state, respectively.

In this paper we describe our efforts to study the electronic structure of nitridoiron(V) species containing truly innocent auxiliary ligands by EPR and Mössbauer spectroscopy. In two recent papers we have shown that 1,4,8,11-tetraazacyclotetradecane (cyclam) complexes of chromium(III)[21] and manganese(III),[22] namely *trans*-[(cyclam)M^{III}(N$_3$)$_2$]$^+$ (M = Cr, Mn), are readily photolyzed with quantitative formation of *trans*-[(cyclam)M^{V}≡N(Y)]$^{n+}$ complexes where Y represents a sixth ligand such as a linear bridging N$_3^-$, CH$_3$CN or ClO$_4^-$, or CF$_3$CO$_2^-$. Here we report the synthesis of *cis*- and *trans*-[(cyclam)Fe^{III}(N$_3$)$_2$](ClO$_4$) and investigate their photochemistry at ambient temperature in solution and at low temperature in frozen solution.

An additional point of interest concerns the product distribution during photolysis in *frozen* solutions. As we pointed out previously,[15] it is difficult to reconcile the product distribution of reported photolysis reactions of azidoiron(III) complexes[1−12] if a nitridoiron(V) species (photooxidation) is the only primary product. The formation of species containing the [Fe(μ-N)Fe]$^{4+}$ core in solution indicates to us that a photo*reduced* ferrous complex must be generated at the same time. Such a species would not have been detected in the RR study of Nakamoto and Wagner.[16,17]

Results and Discussion

Syntheses and Characterization of Ferric Precursor Complexes. The reaction of yellow *cis*-[Fe^{III}(cyclam)Cl$_2$]Cl [23] in an HClO$_4$-acidic methanol/water mixture with an excess NaN$_3$ and heating of the solution to 50 °C yields upon addition of NaClO$_4$ yellow brown, needle-shaped crystals of *trans*-[Fe^{III}(cyclam)(N$_3$)$_2$](ClO$_4$) (**1a**). The same reaction in CH$_3$CN/H$_2$O to which HPF$_6$ had been added produced the corresponding hexafluorophosphate salt (**1b**). When the reaction was carried out at −18 °C red microcrystals of *cis*-[Fe^{III}(cyclam)(N$_3$)$_2$](ClO$_4$) (**2**) were obtained.

In the infrared spectra of **1a** and **2** the *cis*- and *trans*-conformation of the coordinated cyclam ligands are clearly discernible:[24] **2** displays two γ(N−H) wagging bands at 863 and 850 cm^{-1} and two δ(CH$_2$) deformation modes at 806 and 796 cm^{-1}, whereas for **1a** each of these modes exhibits only one band at 886 and 812 cm^{-1}, respectively. In addition, **2** exhibits two ν_{as}(N$_3$) stretching frequencies at 2078 and 2047 cm^{-1}, whereas in **1a** only a single band at 2044 cm^{-1} is observed.[25]

The crystal structures of *trans*-[(cyclam)Fe^{III}(N$_3$)$_2$](PF$_6$) (**1b**) and of *cis*-[(cyclam)Fe^{III}(N$_3$)$_2$](ClO$_4$) (**2**) have been determined by single-crystal X-ray crystallography at 293(2) and 100(2) K, respectively. The structures of the monocations are shown in Figure 1; selected bond distances and angles are given in Table 1.

The structure of **1b** consists of *trans*-[(cyclam)Fe^{III}(N$_3$)$_2$]$^+$ monocations and uncoordinated hexafluorophosphate anions.

(14) Jüstel, T.; Weyhermüller, T.; Wieghardt, K.; Bill, E.; Lengen, M.; Trautwein, A. X.; Hildebrandt, P. *Angew. Chem., Int. Ed. Engl.* **1995**, *34*, 669.
(15) Jüstel, T.; Müller, M.; Weyhermüller, T.; Kressl, C.; Bill, E.; Hildebrandt, P.; Lengen, M.; Grodzicki, M.; Trautwein, A. X.; Nuber, B.; Wieghardt, K. *Chem.—Eur. J.* **1999**, *5*, 793.
(16) Wagner, W.-D.; Nakamoto, K. *J. Am. Chem. Soc.* **1988**, *110*, 4044.
(17) Wagner, W.-D.; Nakamoto, K. *J. Am. Chem. Soc.* **1989**, *111*, 1590.
(18) Groves, J. T.; Takahashi, T.; Butler, W. M. *Inorg. Chem.* **1983**, *22*, 884.
(19) Buchler, J. W.; Dreher, C.; Lay, K. L. *Z. Naturforsch., B: Anorg. Chem., Org. Chem.* **1982**, *37B*, 1155.
(20) Sellmann, D.; Emig, S.; Heinemann, F. W. *Angew. Chem.* **1997**, *109*, 1808; *Angew. Chem., Int. Ed. Engl.* **1997**, *36*, 1734.
(21) Meyer, K.; Bendix, J.; Bill, E.; Weyhermüller, T.; Wieghardt, K. *Inorg. Chem.*, in press.
(22) Meyer, K.; Bendix, J.; Metzler-Nolte, N.; Weyhermüller, T.; Wieghardt, K. *J. Am. Chem. Soc.* **1998**, *120*, 7260.
(23) Chan, P.-K.; Poon, C.-K. *J. Chem. Soc., Dalton Trans.* **1976**, 858.
(24) Poon, C.-K. *Inorg. Chim. Acta* **1970**, *5*, 322.
(25) Czernuszewicz, R. S.; Wagner, W.-D.; Ray, G. B.; Nakamoto, K. *J. Mol. Struct.* **1991**, *242*, 99.

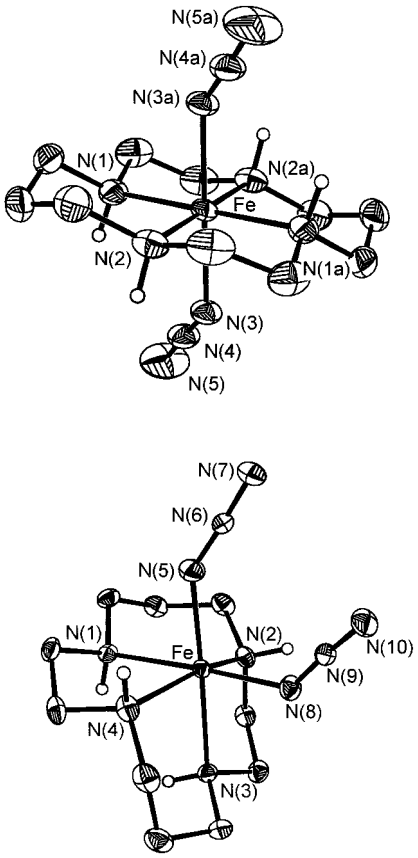

Figure 1. Perspective view and atom labels of the monocations in crystals of **1b** (top) and **2** (bottom). Small open circles represent amine hydrogen atoms.

Table 1. Selected Bond Lengths (Å) and Angles (deg) for **1b** and **2**

1b		**2**	
Fe−N1	2.004(2)	Fe−N1	2.201(2)
Fe−N2	1.998(2)	Fe−N2	2.155(2)
		Fe−N3	2.215(2)
		Fe−N4	2.144(2)
Fe−N3	1.937(2)	Fe−N5	1.976(3)
		Fe−N8	1.970(3)
N3−N4	1.180(3)	N5−N6	1.194(4)
N4−N5	1.145(4)	N6−N7	1.145(4)
		N8−N9	1.210(4)
		N9−N10	1.141(4)
N1−Fe−N2	94.95(10)	N1−Fe−N2	85.83(9)
N2−Fe−N1a	85.05(10)	N2−Fe−N3	79.74(9)
		N3−Fe−N4	84.97(9)
		N4−Fe−N1	79.85(9)
N1−Fe−N1a	180.0	N2−Fe−N4	158.63(10)
N2−Fe−N2a	180.0	N1−Fe−N8	177.08(10)
		N3−Fe−N5	176.78(10)
Fe−N3−N4	129.5(2)	Fe−N5−N6	139.8(2)
N3−N4−N5	176.4(3)	N5−N6−N7	176.4(3)
		Fe−N8−N9	132.0(2)
		N8−N9−N10	176.6(3)

The tetradentate ligand cyclam adopts the most stable *trans*-III configuration.[26] The average $Fe-N_{amine}$ bond length at 2.001(2) Å is typical for such bonds where the central ferric ion has a low-spin d^5 electron configuration. The $Fe-N_{azide}$ bond at 1.937(2) Å is shorter and may indicate some Fe-to-N_3 π-back-donation. Interestingly, in *trans*-[(cyclam)$Mn^{III}(N_3)_2]^+$ containing a high-spin Mn^{III} ion (d^4) the $Mn-N_{azide}$ bonds are longer than the $Mn-N_{amine}$ bonds due to a static Jahn−Teller elongation of the $N_3-Mn^{III}-N_3$ axis.[22] In *trans*-[(cyclam)$Cr(N_3)_2]^+$, on the other hand, the average $Cr-N_{amine}$ bond length is at 2.06 ± 0.01 Å, whereas the two coordinated N_3^- ligands in *trans* position relative to each other are not equivalent: the two Cr−N_3 distances are 2.030(4) and 1.924(4) Å, respectively, but both are shorter than the $Cr-N_{amine}$ bonds.[21] From this we conclude that the observed compressed octahedron in **1b** is not a simple manifestation of the (in principle dynamic) Jahn−Teller effect of a low-spin ferric ion because the resulting ground state ^2E_g would still be degenerate ((d_{xy}^2), $(d_{xz,yz}^3)$). In fact, magnetic susceptibility and EPR measurements given below show that the electronic ground state of **1b** is nondegenerate and without first-order orbital magnetic moment as in a $^2B_{2g}$ ($(d_{xz,yz})^4$ $(d_{xy})^1$) rather than an ^2E_g ground state. The ligand-field picture that could be anticipated from the molecular geometry must therefore be corrected for covalent bond effects from the axial ligands which render the (*xz*),(*yz*) d-orbitals lower in energy than the (*xy*)-orbital.

The structure of **2** consists of *cis*-[(cyclam)$Fe^{III}(N_3)_2]^+$ monocations and uncoordinated perchlorate anions. Two $Fe-N_{amine}$ bond distances in *trans* position relative to each other at 2.150(2) Å are shorter than the corresponding two in *cis* position at 2.208(2) Å. This reflects the *trans*-influence of the two azido ligands (average $Fe-N_{azide}$ 1.973(3) Å). Both the $Fe-N_{amine}$ and the $Fe-N_{azide}$ bond distances in **2** are significantly longer than those in **1b**. This is due to an increased ionic radius of the high-spin ferric ion in **2** (0.785 Å) as compared to the low-spin Fe^{III} ion in **1b** (0.69 Å).

From temperature-dependent magnetic susceptibility measurements on a powdered sample of **2** a nearly temperature-independent magnetic moment of 5.89 μ_B at 290 K (5.77 μ_B at 50 K) was found in excellent agreement with the spin-only value of 5.92 μ_B for an octahedral high-spin ferric ion. A spin-Hamiltonian simulation ($S = {}^5/_2$) of the magnetic data recorded in the range 2−300 K yielded a zero-field splitting parameter $|D| = 1.1$ cm^{-1} and $g = 2.0$. In contrast, the magnetic moment of **1b** is 2.39 μ_B at 298 K. Its temperature dependence (2−300 K) was simulated with $S = {}^1/_2$ and $g = 2.27$. This is indicative of a low-spin octahedral ferric ion. The observations are in line[23] with other *cis*/*trans*-[(cyclam)$Fe^{III}(Y)_2]^+$ complexes, e.g., for X = Cl, NCS^-, where the *cis*-isomers contain a high-spin Fe^{III} and the corresponding *trans* complexes are low-spin.

The X-band EPR spectra of **1a** and **2** in CH_3CN solution at 4 K are in agreement with the presence of low- and high-spin configurated Fe^{III} ions, respectively. Figure 2 shows these spectra. The spectrum of **1a** is apparently one of axial symmetry but simulations with rhombic *g*-values $g_1 = 2.40$, $g_2 = 2.31$, and $g_3 = 1.91$ give a better fit, which is in accord with the 2-fold rotation symmetry of cyclam and the bent axial azide ligands. The *g*-values can be explained in the crystal field model for spin−orbit interaction of distorted low-spin $(t_{2g})^5$ complexes developed by Griffith[27] and extended by Taylor.[28] This model shows that **1a** has a $(d_{xz}, d_{yz})^4(d_{xy})^1$ ground state with the unpaired spin being in the almost pure (*xy*)-orbital (99%). Two physically equivalent solutions can be found for the assignments of **g** tensor components in a "proper axis system" ($V/\Delta < 2/3$),[28] $\bar{g} = (-2.40, 2.31, -1.91)$ or $\bar{g} = (-2.31, 2.40, -1.91)$, where only the *x* and *y* components are interchanged. From the *g*-values we find orbital mixing coefficients of 0.085(*yz*), 0.103(*xz*), and 0.995(*xy*) (or (*yz*) and (*xz*) interchanged). The corresponding

(26) (a) Bosnich, B.; Poon, C.-K.; Tobe, M. L. *Inorg. Chem.* **1965**, *4*, 1102. (b) Adam, K. R.; Atkinson, I. M.; Lindoy, L. F. *Inorg. Chem.* **1997**, *36*, 480.

(27) Griffith, J. S. *Proc. R. Soc. London, A* **1956**, *235*, 23−36.
(28) Taylor, C. P. S. *Biochim. Biophys. Acta*, **1977**, *491*, 137.

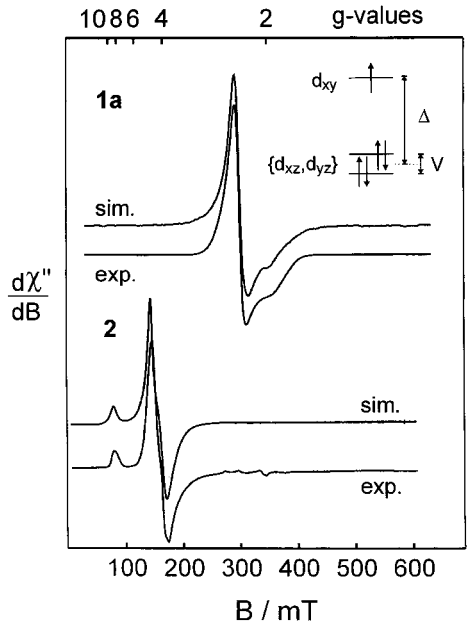

Figure 2. X-band EPR spectra of **1a** (top) and **2** (bottom) in frozen CH_3CN at 4 and 3 K, respectively. Experimental conditions: **1a** microwave frequency 9.64 GHz, microwave power 100 μW, modulation amplitude 1 mT; **2** 9.65 GHz, 252 μW, 1.4 mT. The simulations are powder calculations performed with (effective) *g*-values. **1a** $\bar{g} = (2.40, 2.31, 1.91)$, anisotropic line widths $\bar{W} = (26.2, 25.2, 6.6)$ mT (Lorentzians); **2** superposition (1:1) of two subspectra (Kramers doublets of $S = {}^5/_2$) with $\bar{g}_1' = (8.7, 0.5, 0.5)$ $\bar{W}_1 = (7.0, 7.0, 7.0)$ mT and $\bar{g}_2' = (4.13, 3.95, 4.70)$, $\bar{W}_2 = (25., 10., 4.5)$ mT. The inset shows the ligand-field splittings of t_{2g} orbitals for **1a**.

energy splittings of the t_{2g} orbitals have a strong tetragonal part $\Delta/\lambda = -5.76$ as well as a significant rhombic contribution $|V/\lambda| = 1.29$, where λ is the spin−orbit coupling constant. The negative sign for Δ indicates that d_{xy} is higher in energy than the doublet (d_{xz}, d_{yz}) (see inset in Figure 2).

The EPR spectrum of **2** exhibits two features at $g' \approx 9$ and ≈ 4.3, which were successfully simulated with the following two sets of effective *g*-values for the zero-field split Kramers doublets of a rhombic $S = {}^5/_2$ system with $E/D = 0.26$: $g_x' = 3.95$, $g_y' = 4.13$, $g_z' = 4.70$ and $g_y' = 8.70$, $g_x' = g_z' = 0.5$. Spectral differences of lowest and highest Kramers doublets with the resonances close to $g' = 9$ are not resolved due to the close similarity of both doublets at $E/D \approx {}^1/_3$. From the intensity variation of the $g' = 4.3$ signal of the middle Kramers doublet measured in the range 2−30 K, a zero-field splitting parameter $|D| = 1.1 \pm 0.3$ cm^{-1} has been determined in accordance with the magnetic data. This value is below the typical range 3−15 cm^{-1} found for *D* values of (five-coordinate) high-spin iron(III) in porphyrins.[29] As the zero-field splitting of the $^6A_1$ ground state in a simple picture[30,31] is due to spin−orbit coupling with the first excited quartet term $^4A_2$ the low *D* value and the correspondingly large $^6A_1/^4A_2$ splitting reflect a much lower 10 *Dq* splitting of e_g and t_{2g} levels in the asymmetric iron moiety of the *cis*-isomer than in the *trans*-isomer where the iron ion experiences a strong ligand field in the plane of cyclam.

The zero-field Mössbauer spectra of **1a** and **2** are shown in Figure 3 (top), and Table 2 summarizes the data. The spectrum of **1a** in CH_3CN at 80 K displays a single quadrupole doublet with an isomer shift, δ, of 0.29 mm s^{-1}, a large quadrupole splitting, ΔE_Q, of 2.26 mm s^{-1}, and a line-width, Γ, of 0.29 mm s^{-1}. In contrast, for **2** dissolved in CH_3CN a quadrupole doublet with small splitting is observed at 80 K: $\delta = 0.46$ mm s^{-1}, $\Delta E_Q = 0.29$ mm s^{-1}, $\Gamma = 1.07(5)$ mm s^{-1}. These isomer shift values are typical for low- and high-spin octahedral iron(III) complexes, respectively. The small quadrupole splitting of **2** reflects the "spherical" symmetry of the $(t_{2g})^3(e_g)^2$ configuration, whereas the large splitting for **1a** results from the large orbital contribution to the electric field gradient (efg) tensor for a $(t_{2g})^5$ configuration.

Magnetic Mössbauer measurements of **1a** at 160 K with 7 T applied field (Figure 4A) revealed a negative sign of V_{zz}, the main component of the efg, and a moderately strong asymmetry parameter $\eta = V_{xx} - V_{yy}/V_{zz}$ of 0.4. This is consistent with the assumption that the d_{xy} orbital is the half-filled orbital in **1a** as deduced above from the EPR *g*-values. The t_{2g} hole model with $\Delta/\lambda = -5.76$ and $V/\lambda = -1.29$ predicts a valence contribution to the electric quadrupole splitting of $\Delta E_Q = -2.94$ mm s^{-1} and $\eta = 0.01$. Here it has been assumed that a single "hole" in a pure d_{xy} eigenstate produces a quadrupole splitting of −4.2 mm s^{-1}.[32] Since this factor depends on the radial distribution $<r^{-3}>$, where the average for $t_{2g}{}^5$ includes all 3d electrons, the deviation from experiment ($\Delta E_Q = -2.26$ mm s^{-1}) indicates charge delocalization due to covalent bonds.

Application of 3−7 T magnetic fields at liquid helium temperatures resolves the magnetic hyperfine splitting of solid **1a** as shown in Figure 4B. The asymmetry of the spectra is typical of a highly anisotropic hyperfine coupling tensor and resembles those of low-spin ferri-porphyrinates.[29,33,34] Spin-Hamiltonian simulations yield a coupling tensor $\bar{\mathbf{A}}/g_N\beta_N = (+2.29, -6.26, -25.39)$ T with the other parameters set to the values determined from the measurements at 80 and 160 K or from EPR. Considerable improvement of the fit was achieved when the efg tensor was allowed to have a different orientation than $\bar{\mathbf{A}}$ and **g** tensors so that $V_{z'z'}$ was found almost along A_{yy} (Euler angles, $\beta = 78°$, $\gamma = 90°$). This shows that covalency and lattice contributions to the efg cannot be neglected.

The signs and the symmetry of the $\bar{\mathbf{A}}$ tensor components, however, are again consistent with the d_{xy} hole description of **1a**. Taking the orbital coefficients from the EPR analysis one can calculate the Fermi contact, orbital and spin-dipolar contributions to $\bar{\mathbf{A}}$.[34−36] With the orbital reduction factor set to $k = 1$ and the factor of the Fermi contact term assumed to be $\kappa = 0.35$ we find $\bar{\mathbf{A}}/g_N\beta_N = \mathrm{P}\,(0.27, -0.19, -0.79)$ T. As *P* is depending on the "hole" distribution, we treated it as a scaling factor which accounts for delocalization of the "hole" spin over 3d and ligand orbitals. The best match of the experimental $\bar{\mathbf{A}}$ tensor is found with $P = 30.1$ T and the corresponding prediction values $\bar{\mathbf{A}}/g_N\beta_N = (8.26, -5.60, -23.64)$ T, which is in reasonable agreement with the experiment and shows that EPR and magnetic Mössbauer spectra yield a consistent

(29) Debrunner, P. G. Mössbauer Spectroscopy of Iron Porphyrins. In *Iron Porphyrins*; Lever, A. B. P., Gray, H. B., Eds.; VCH: Weinheim, 1989; Vol. III, p 137.

(30) (a)Maltempo, M. M.; Moss, T. H. *Quart. Rev. Biophys.* **1976**, *9*, 181−215. (b) Maltempo, M. M. *J. Chem. Phys.* **1974**, *61*, 2540−2547.

(31) Neese, F.; Solomon, E. I. *Inorg. Chem.* **1998**, *37*, 6568−6582.

(32) The valence contribution from an electron in a hypothetical pure d_{xy} orbital would yield $E_Q = +4.2$ mms^{-1}, by taking $<r^{-3}> = 5\ a_0{}^{-3}$ and $Q = 0.15$ b and neglecting covalency and lattice contribution to the efg; (a) Bominaar, E. L.; Guillin, J.; Sawaryn, A.; Trautwein, A. X. *Phys. Rev. B* **1989**, *39*, 72.; (b) Lauer, S.; Marathe, V. R.; Trautwein, A. X. *Phys. Rev. A* **1979**, *19*, 1852.

(33) Walker, F. A.; Nasri, H.; Turowska-Tyrk, I.; Mohanrao, K.; Watson, C. T.; Shokhirev, N. V.; Debrunner, P. G.; Scheidt, W. R. *J. Am. Chem. Soc.* **1996**, *118*, 12109−12118.

(34) (a) Safo, M. K.; Gupta, G. P.; Walker, F. A.; Scheidt, W. R. *J. Am. Chem. Soc.* **1991**, *113*, 5497−5510. (b) Walker, F. A.; Huynh, B. H.; Scheidt, W. R.; Osvath, S. R. *J. Am. Chem. Soc.* **1986**, *108*, 5288−5297.

(35) Oosterhuis, W. T.; Lang, G. *Phys. Rev.* **1969**, *178*, 439−456.

(36) Lang, G.; Marshall, W. *Proc. Phys. Soc.* **1966**, *87*, 3−34.

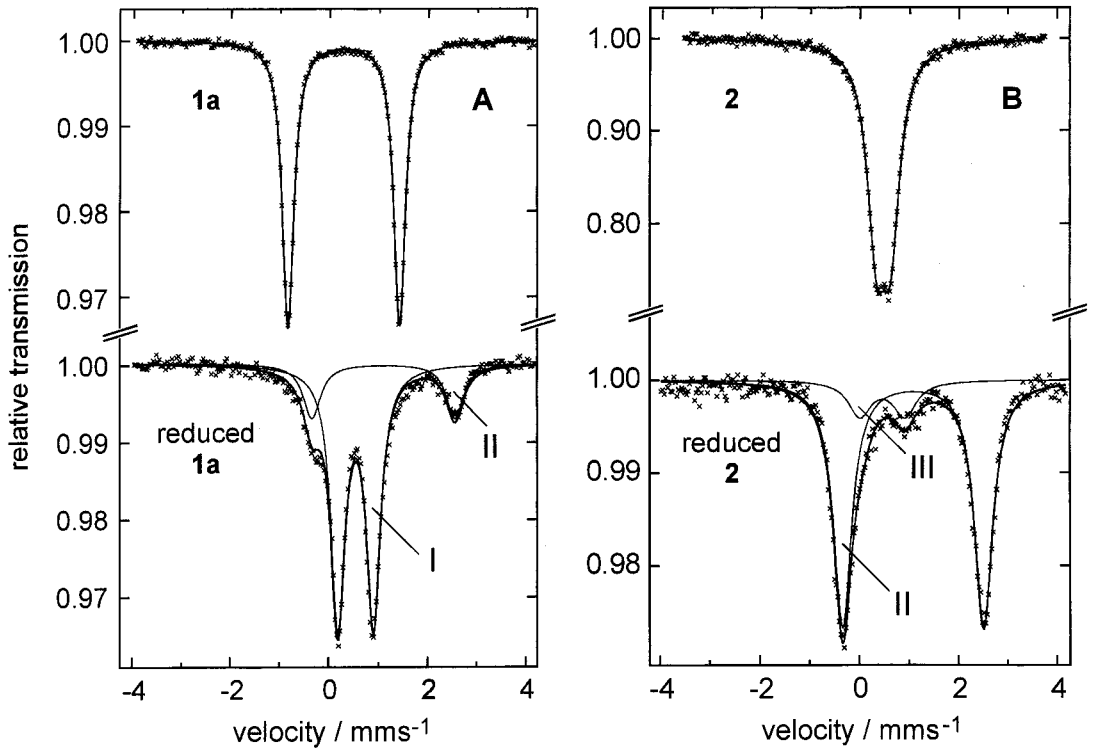

Figure 3. Zero-field Mössbauer spectra of 35% ^{57}Fe-enriched **1a** (80 K, 1.5 mM CH_3CN) and **2** (3 K, solid) and their electrochemically one-electron reduced CH_3CN solutions (80 K, 1.5 mM). The sample of reduced **1a** (A, bottom) was immediately frozen after Coulometric reduction at -30 °C. Samples taken after prolonged incubation in solution at −30 °C showed strong enhancement of subspectrum II and concomitant attenuation of I. Subspectrum III in (B) with $\delta = 0.49$ mm s^{-1}, $\Delta E_Q = 0.90$ mm s^{-1} is most probably an $[Fe^{III}-O-Fe^{III}]^{4+}$ contamination. This spectrum was exclusively obtained when a reduced sample of **2** was oxidized by air.

Table 2. Mössbauer Data of Ferric and Ferrous Complexes

complex		T, K	δ, mm s^{-1}	ΔE_Q, mm s^{-1}	Γ, mm s^{-1}
1a	CH_3CN	80	0.29(5)	2.26(1)	0.29(2)
	powder	80	0.28(6)	2.24(1)	0.27(1)
2	CH_3CN	80	0.46(2)	0.29(3)	1.07(5)
	powder	3	0.49(5)	0.26(1)	0.45(5)
trans-[(cyclam)$Fe^{II}(N_3)_2$]	CH_3CN	80	0.55(7)	0.72(4)	0.34(4)
cis-[(cyclam)$Fe^{II}(N_3)_2$]	CH_3CN	80	1.11(7)	2.84(1)	0.45(1)

description of **1a** as a low-spin ferric complex with $(d_{xz}, d_{yz})^4(d_{xy})^1$ ground state.

Recently the conditions for stabilization of the $(d_{xz}, d_{yz})^4(d_{xy})^1$ ground states, instead of the more common $(d_{xy})^2(d_{xz}, d_{yz})^3$ configuration, were systematically investigated for low-spin ferri-porphyrinates.[33,34,37] It was found that strong axial π-acceptors induce significant ruffling of the porphyrins which could be attributed to mixing of iron d_{xy} and porphyrin $a_{2u}(\pi)$ orbitals. The orbital mixing is made possible by the twist of nitrogen p_z orbitals out of the porphyrin mean plane. The π-donation from the equatorial ligands changes the orbital energies markedly in that d_{xy} becomes higher in energy than the d_{xz}, d_{yz} pair. In contrast, cyclam in the *trans*-III configuration is a pure σ donor and, therefore, the above analysis does not apply for **1a**.

Characterization of Ferrous Complexes. The electrochemistry of **1a** and **2** in CH_3CN (0.10 M [N(*n*-butyl)$_4$]PF_6 supporting electrolyte) has been studied by cyclic and square-wave voltammetry. The potentials given are referenced versus the ferrocenium/ferrocene (Fc^+/Fc) couple. Both species exhibit a reversible, metal-centered one-electron reduction wave at −0.76 V for **1a** and −0.62 V for **2** at 20 °C (scan rate: 200 mV s^{-1}). In addition, both complexes exhibit an irreversible oxidation wave of +0.84 V which is assigned to the irreversible oxidation of uncoordinated azide yielding the azide radical which rapidly decomposes with formation of N_2.

Considering the differing cavity size of coordinated *trans*- and *cis*-cyclam ligands we anticipated that *trans*-[(cyclam)$Fe^{II}(N_3)_2$] is low-spin, whereas *cis*-[(cyclam)$Fe^{II}(N_3)_2$] is high-spin. This has been proven by Mössbauer spectroscopy. An electrochemically generated sample of reduced **1a** with 35% enriched ^{57}Fe showed two subspectra at 80 K: A major doublet I (80% relative intensity) at $\delta = 0.55$ mm s^{-1} and $\Delta E_Q = 0.72$ mm s^{-1} has been observed (Figure 3A, bottom). These values are typical for octahedral low-spin ferrous complexes ($(t_{2g})^6$ configuration, $S = 0$). In addition, a weaker (20%) subspectrum II at $\delta = 1.11$ mm s^{-1} and $\Delta E_Q = 2.92$ mm s^{-1} has been observed which corresponds to a high-spin *cis*-[(cyclam)$Fe^{II}(N_3)_2$] species ($S = 2$). A similar spectrum of the latter species has been obtained from electrochemically one-electron reduced **2** in CH_3CN at 80 K: $\delta = 1.11$ mm s^{-1}, $\Delta E_Q = 2.84$ mm s^{-1} (Figure 3B, bottom). This shows that CH_3CN solutions of *trans*-[(cyclam)$Fe^{II}(N_3)_2$] are not stable. The *trans* → cis isomerization was also followed by the appearance and gradual growing-in of the current peak characteristic for *cis*-[(cyclam)$Fe^{II}(N_3)_2$] at −0.62 V in square-wave voltammograms recorded after coulometric reduction of **1a**. At −30 °C the slow *trans* → cis isomerization is complete within ∼1 h.

Photolyses at −35 and 20 °C. Figure 5 shows the electronic spectra of **1a** and **2** in CH_3CN solution at ambient temperature

(37) (a) Safo, M. K.; Walker, F. A.; Raitsimring, A. M.; Walters, W. P.; Dolata, D. P.; Debrunner, P. G.; Scheidt, W. R. *J. Am. Chem. Soc.* **1994**, *116*, 7760−7770. (b) Inniss, D.; Soltis, S. M.; Strouse, C. E. *J. Am. Chem. Soc.* **1988**, *110*, 5644−5650. (c) Soltis, S. M.; Strouse, C. E. *J. Am. Chem. Soc.* **1988**, *110*, 2824−2829. (d) Quinn, R.; Valentine, J. S.; Byrn, M. P.; Strouse, C. E. *J. Am. Chem. Soc.* **1987**, *109*, 3301−3308 and references therein.

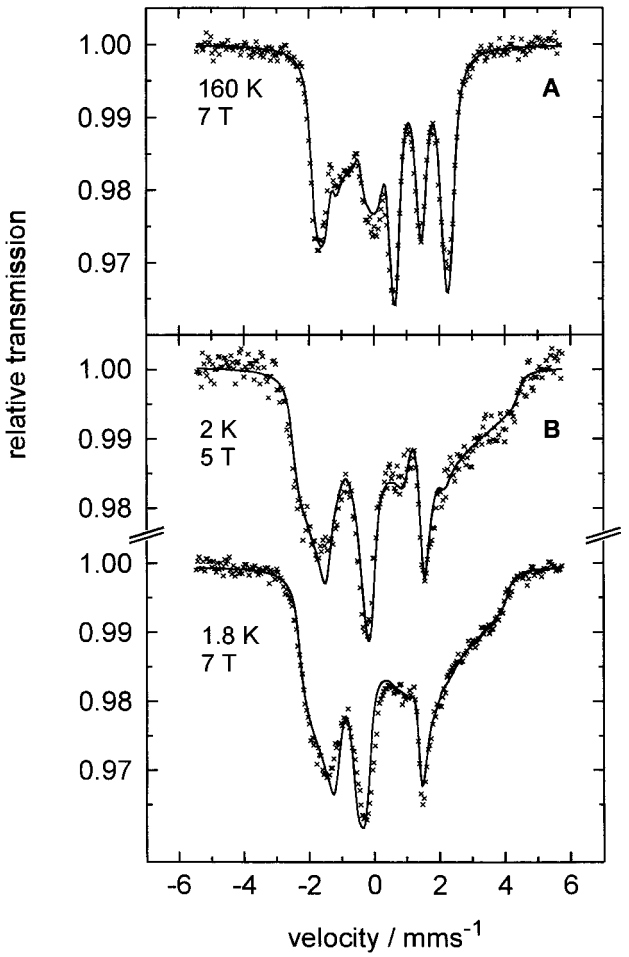

Figure 4. Magnetically perturbed Mössbauer spectra of **1a** with the indicated fields applied perpendicular to the γ-beam. The sample was as that used for Figure 3A, top. The solid lines are the result of a spin-Hamiltonian simulation as decribed in the text.

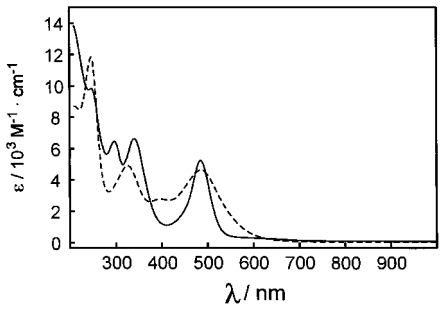

Figure 5. Electronic spectra of **1a** (—) and **2** (- — -) in CH_3CN solution at 297 K.

and Table 3 summarizes the data. Both spectra are dominated by intense charge-transfer bands in the ultraviolet and visible region.

When a deep-red solution of **2** in deaerated (Ar-blanketing atmosphere), dry acetonitrile was photolyzed with a Hg immersion lamp at −35 °C, a color change to bright yellow was observed within 60 min. Figure 6 shows the spectral changes observed as a function of time. During this process the intense CT bands of **2** at 487 and 247 nm lose intensity, and concomitantly, the CT band at 327 nm is shifted bathochromically by 13 nm. Three isosbestic points at ∼400, 250, and ∼220 nm are observed.

We have followed the course of this photolysis by measuring the EPR spectra at 4 K of samples taken 10, 40, and 60 min after the illumination was started. At the beginning the rhombic signal of the starting complex **2** is the only EPR active species in solution; this signal gradually disappears upon illumination and a new, well-resolved signal at higher field builds up. After 60 min of illumination this new axial signal is observed as the dominant spectral feature (95%) at effective g-values of $g_{x,y}' \approx 4$ and $g_z' \approx 2$. Figure 7A shows the corresponding spectrum of a sample which was enriched with ^{57}Fe for subsequent Mössbauer measurements. An excellent simulation of the EPR spectrum was achieved with effective g-values $g_x' = 3.85$, $g_y' = 4.05$, $g_z' = 2.0$. These values are typical of a spin quartet species with nearly axial symmetry ($E/D = 0.02$)[38] and dominating zero-field splitting ($D \gg h\nu \approx 0.3$ cm^{-1} at X-band). The EPR-transitions occur only within the Kramers doublets and the effective g-values for $|S, \pm 1/2>$ are $g_x' \cong g_y' = g_\perp(S+1/2)$, $g_z' = g_{||}$, where $g_\perp$ and $g_{||}$ are the intrinsic g factors of the Zeeman interaction.[39] The powder spectrum of $|S,\pm 3/2>$ is highly anisotropic for $E/D \approx 0$ and therefore not observable. Our results are consistent with $S = 3/2$ and $g_\perp \approx g_{||} \approx g_e$. For $D > 0$ the EPR silent $|S,\pm 3/2>$ doublet is $2D$ above the ground state. From the temperature dependence of the EPR intensity of the $g' \approx 4$ signal we found $D = +9(\pm 3)$ cm^{-1} (for details see ref 15). Very similar EPR spectra have recently been reported[14,15] for a series of dinuclear, mixed-valent complexes containing the linear $[Fe^{III}(\mu\text{-N})Fe^{IV}]^{4+}$ core (Table 4). For these complexes strong intramolecular antiferromagnetic coupling between a high-spin ferric ($S = 5/2$) and a low-spin Fe^{IV} ($S = 1$) ion has been observed yielding an $S_t = 3/2$ ground state. Thus we propose that photolysis of **2** yields the dinuclear μ-nitrido bridged species $[\{(cyclam)Fe(N_3)\}_2(\mu\text{-N})]^{2+}$.

We have also recorded the Mössbauer spectrum of the yellow acetonitrile solution of **2** (35% enriched ^{57}Fe) which had been illuminated for 60 min at −35 °C. The spectrum recorded at 80 K is shown in Figure 8A. The spectrum was satisfactorily fitted by three subspectra: (a) an intense symmetric quadrupole doublet $\delta = 0.14$ mm s^{-1}, $\Delta E_Q = 0.79$ mm s^{-1} (46% rel intensity), (b) an asymmetric doublet at $\delta = 0.47$ mm s^{-1}, and $\Delta E_Q = 1.89$ mm s^{-1} (47% rel intensity), and (c) a minor doublet (7% rel intensity) at fixed parameters $\delta = 0.46$ mm s^{-1}, $\Delta E_Q = 0.29$ mm s^{-1} which corresponds to that of the starting material **2**.

Three observations are remarkable: (i) The areas of subspectra a and b add up to 93% conversion of **2** into the dinuclear species; only ∼7% of the starting material is present. (ii) Only a high-spin ferric ($S = 5/2$, subspectrum b) and an Fe^{IV} ($S = 1$, subspectrum a) ion (ratio 1:1) are photolytically generated. Their Mössbauer parameters summarized in Table 5 are very similar to those reported for other isolated and crystallographically characterized species containing the mixed-valent $[Fe^{III}(\mu\text{-N})Fe^{IV}]^{4+}$ ($S_t = 3/2$) core with (on the time scale of a Mössbauer experiment (∼10^{-7} s)) localized valencies at the iron ions (class I or II). (iii) No indication for the formation of ferrous or Fe^V ions during the photolysis of **2** at −35 °C has been detected.

The line asymmetry of the high-spin ferric subspectrum b in Figure 8A indicates magnetic broadening due to "intermediate" spin relaxation. The effect is much stronger for the ferric than for the Fe^{IV} site, presumably because of the larger effective hyperfine coupling components of Fe^{III} (see below). In strong applied fields (3−7 T) the relaxation rate decreases so that at low temperatures (2.5−15 K) the Mössbauer doublets split magnetically (Figure 9). Spin-Hamiltonian simulations per-

(38) Derived from the first-order perturbation expression for $S = 3/2$: $E/D = 1/12\ |g_x - g_y|$.

(39) Trautwein, A. X.; Bill, E.; Bominaar, E. L.; Winkler, H. *Struct. Bonding* **1991**, *78*, 1−95.

Table 3. Electronic Spectra of Complexes in CH_3CN Solution

complex	λ_{max}, nm (ϵ, L mol^{-1}cm^{-1})[a]
1a	248(9.8×10^3), 298(6.4×10^3), 342(6.5×10^3), 487(5.2×10^3)
yellow solution after 15 min photolysis	395(2.9×10^3)
2	247(1.2×10^4), 327(5.0×10^3), 399(3.0×10^3), 486(4.8×10^3)
yellow solution after 60 min photolysis	340(6.1×10^3), ~410(3.8×10^3)sh

[a] Molar absorption coefficients are all calculated per iron ion.

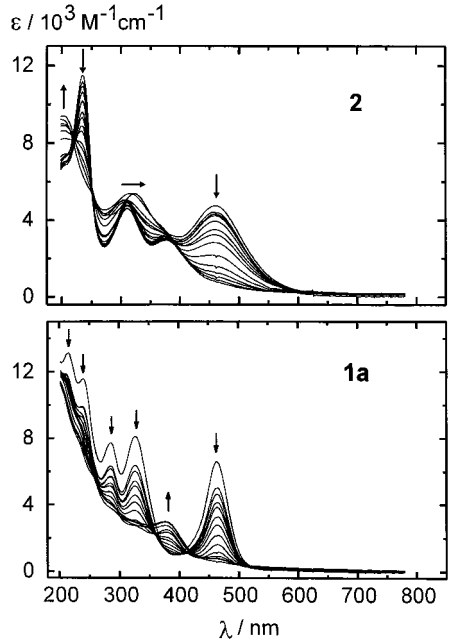

Figure 6. Spectral changes observed during photolysis of **2** (top) and **1a** (bottom) in CH_3CN solution at −20 and +20 °C, respectively. Spectra for **2** were recorded in 4-min intervals and those for **1a** in 1-min intervals. The isosbestic points appear ill-defined due to solvent evaporation during photolysis caused by passing Ar through the solution.

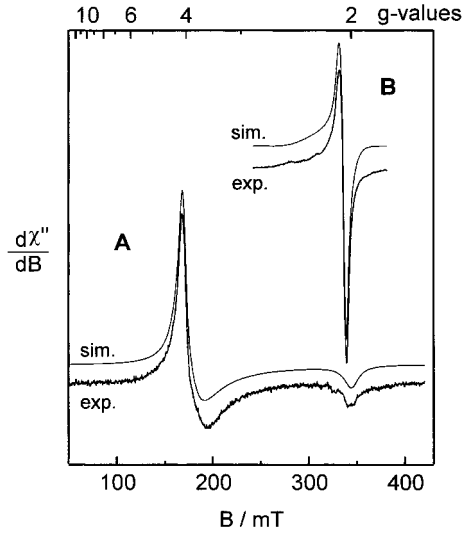

Figure 7. X-band EPR spectra (10 K) of **2** in CH_3CN (1.7 mM) after 60 min of photolysis at −35 °C (A) and **1a** in CH_3CN (1.7 mM) after 15 min of irradiation at 20 °C (B). The samples were aliquots of the preparations used for the corresponding Mössbauer spectra shown in Figures 8 and 9 or 10. Experimental conditions: microwave frequency 9.6439 GHz (A)/9.6445 GHz (B); power 2 μW (A)/1 μW (B); modulation amplitude 1.2 mT. The simulations are performed with (effective) *g*-values: (A) $\bar{g}' = (3.85, 4.05, 2.0)$, Lorentzian lines $\bar{W} =$ (10., 39., 20.) mT; (B) $\bar{g}' = (2.04, 2.06, 2.20)$, Gaussian lines $\bar{W} =$ (4.4, 6.9, 36.) mT.

formed with the total spin $S_t = {}^3/_2$ allowed us to assign individual subspectra in the hyperfine pattern and to determine the signs and magnitudes of efg and $\bar{\mathbf{A}}$ tensors; the parameters are summarized in Table 6.

The weak, widely split lines at about ±7 mm s^{-1} clearly belong to a magnetic sextet with isomer shift, quadrupole splitting, and relative weight according to the minor subspectrum c from above (Figure 8A). Its contribution which was assigned to contaminating ferric starting material (**2**), is a typical $S = {}^5/_2$ hyperfine spectrum with rhombic ZFS ($E/D = {}^1/_3$), isotropic coupling constant $A = -20.6$ T, positive V_{zz}, and small asymmetry parameter $\eta = 0.1$. We claim that these parameters characterize the *cis*-[(cyclam)Fe^{III}(N$_3$)$_2$]$^+$ complex (**2**).

The magnetic properties to the major subspectra a and b in Figure 9 confirm the EPR interpretation that the photolysis product of **2** is a spin-coupled dimer of Fe^{IV} and Fe^{III}. The field-dependence of both species is determined by effective hyperfine coupling components (Table 6, isotropic parts) that show opposite signs, as it is expected for antiferromagnetically coupled sites with local spins aligned antiparallel and parallel to the total spin. The series of spectra was consistently simulated with ZFS parameters *D* and *E*/*D* taken from EPR and thus confirms these values. It should be mentioned that due to the anisotropy of the electronic $|{}^3/_2, \pm{}^1/_2>$ ground-state Kramers doublet which exhibits an "easy plane" of magnetization for fields applied in *x*/*y* orientations,[39] the *x*- and *y*-components of the hyperfine coupling tensors are much better determined than the *z*-components.

For strong spin coupling ($J \gg D$, $g\mu_B\mathbf{B}$) as it can be expected for μ-nitrido dimers, the effective $\bar{\mathbf{A}}$ tensors of Fe^{IV} and Fe^{III} for the total spin $S_t = {}^3/_2$ can be rewritten in the intrinsic representation for the local electronic spins by using eq 9 (Experimental Section). With the values summarized in Table 6 one obtains $\bar{\mathbf{A}}$(Fe^{IV})/$g_N\beta_N$ = (−9.95, −10.45, − 1.17) T and $\bar{\mathbf{A}}$(Fe^{III})/$g_N\beta_N$ = (−13.5, −14.45, −22.7) T.

The magnitude of the isotropic component for Fe^{III} (−16.88 T) is significantly lower than the limit −22T for ionic high-spin ferric compounds. This deviation, as well as the large anisotropy of $\bar{\mathbf{A}}$(Fe^{III}), indicates significant spin-dipolar contributions that originate from covalent spin delocalization. Also the very large quadrupole splitting of Fe^{III} indicates the influence of covalency (the valence contribution to the efg from a "spherical" half-filled 3d^5 shell with ionic ligands would be vanishing).

Isomer shift and quadrupole parameters of the Fe^{IV} site in the photolysis product of **2** resemble those of Fe^{IV}═O species in biological and synthetic porphyrin,[29,40] lactone, and chlorin[41]

(40) (a) Moss, T.; Ehrenberg, A.; Bearden, A. J. *Biochemistry* **1969**, *8*, 4159−4162. (b) Schulz, C. E.; Rutter, R.; Sage, J. T.; Debrunner, P. G.; Hager, L. P. *Biochemistry* **1984**, *23*, 4743−4754. (c) Mandon, D.; Weiss, R.; Jayaraj, K.; Gold, A.; Terner, J.; Bill, E.; Trautwein, A. X. *Inorg. Chem.* **1992**, *31*, 4404−4409 and references therein.

(41) (a) Jayaraj, K.; Gold, A.; Austin, R. N.; Ball, L. M.; Terner, J.; Mandon, D.; Weiss, R.; Fischer, J.; DeCian, A.; Bill, E.; Müther, M.; Schünemann, V.; Trautwein, A. X. *Inorg. Chem.* **1997**, *36*, 4555−4566. (b) Jayaraj, K.; Gold, A.; Austin, R. N.; Mandon, D.; Weiss, R.; Terner, J.; Bill, E.; Müther, M.; Trautwein, A. X. *J. Am. Chem. Soc.* **1995**, *117*, 9079−9080 and references therein.

Table 4. EPR Spectra of Complexes Containing the $[Fe^{III}(\mu\text{-}N)Fe^{IV}]^{4+}$ Core

complex[a]	S_t[b]	g_x'	g_y'	g_z'	D, cm^{-1}	ref
$[\{LFe(Cl_4\text{-cat})\}_2(\mu\text{-N})]$	$^3/_2$	3.99	4.14	2.00	13 ± 5	14
$[\{LFe(nadiol)\}_2(\mu\text{-N})]$	$^3/_2$	4.00	4.12	2.00	7 ± 3	15
$[\{LFe(Ph_2acac)\}(\mu\text{-N})$ $FeL(Cl_4\text{-cat})]^+$	$^3/_2$	3.96	4.07	1.98	21 ± 5	15
$[\{(cyclam)Fe(N_3)\}_2(\mu\text{-N})]^{2+}$	$^3/_2$	3.85	4.05	2.00	9 ± 3	this work
$[\{(tpp)Fe\}_2(\mu\text{-N})]$	$^1/_2$	2.15		2.01		4
$[\{(pc)Fe\}_2(\mu\text{-N})]$	$^1/_2$	2.13		2.03		8
$[(tpp)Fe(\mu\text{-N})Fe(pc)]$	$^1/_2$	2.10		2.005		11
$[\{trans\text{-}(cyclam)(N_3)Fe\}_2(\mu\text{-N})]^{2+}$	$^1/_2$	2.04	2.06	2.20		this work

[a] Ligand abbreviations: Cl_4-cat = tetrachlorocatecholate(2−), L = 1,4,7-trimethyl-1,4,7-triazacyclononane, nadiol = naphthaline-2,3-diolate(2−), Ph_2acac = 1,3-diphenylpropane-1,3-dionate(2−), tpp = tetraphenylporphinate(2−), pc = phthalocyaninate(2−). [b] Ground state of complex.

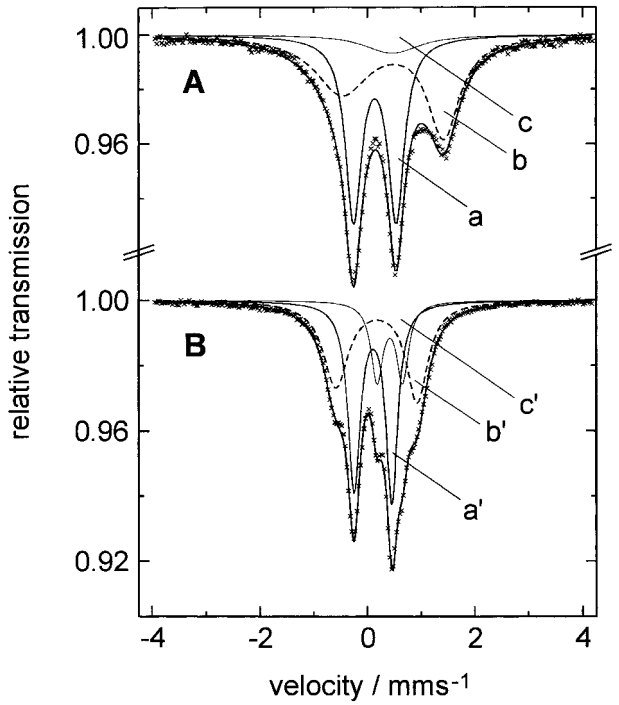

Figure 8. Zero-field Mössbauer spectrum (80 K) of ^{57}Fe-enriched (35%) **2** in CH_3CN (1.7 mM) after 60 min of photolysis at −35 °C (A) and **1a** in CH_3CN (1.7 mM) after 15 min of irradiation at 20 °C (B). The fit (bold solid line) in (A) was obtained by three subspectra: low-spin Fe^{IV} (a), high-spin Fe^{III} (asymmetric line widths) (b), and an impurity of 7% starting material **2** (c). In (B) the subspectra are low-spin Fe^{IV} a′, low-spin Fe^{III} b′, and 18% low-spin Fe^{II} c′.

systems. Particularly the positive sign of V_{zz} is consistent with the low-spin t_{2g}^4 configuration and a low lying d_{xy} orbital as it is found there. In a ligand field picture of the $(d_{xy})^2(d_{xz})^1(d_{yz})^1$ ground state the (positive) valence contribution to the efg can be described by the effect of two electron "holes" in (d_{xz},d_{yz}) and the orbital mixing due to spin−orbital interaction.[42,43] The magnitude of the quadrupole splitting however is usually overestimated in this picture. With reasonable assumptions for tetragonal crystal field splittings one expects quadrupole splittings of about 2 mm s^{-1}, whereas the experimental value is less than half of that. Due to the spin−orbit coupling the Fe^{IV} spin triplet of the Fe^{IV}═O species shows large zero-field splitting on the order of 10 cm^{-1}. This value, however, is in the spin-coupled $[Fe^{III}(\mu\text{-}N)Fe^{IV}]^{4+}$ dimers from photolyzed **2** practically not measurable because the spin projection factor for *D* of the Fe^{IV} site is only $^2/_{30}$ in the magnetic ground state. Its influence on the ZFS of the cluster spin multiplet is therefore only marginal. The magnitudes of V_{zz} and the $\bar{\mathbf{A}}$ tensor components of Fe^{IV} are smaller than for most of the oxo-ferryl (porpyhrin) systems. They match however well with the data of the μ-nitrido Fe^{III}−N−Fe^{IV} (non-heme) dimer complex published recently.[14,15] In that study we found from molecular orbital calculations (spin-polarized self-consistent charge X_α method), that considerable spin and charge delocalization occurs between Fe^{IV} and the μ-N bridge. The relative small positive values of the quadrupole splitting could be particularly well-explained in this scheme, which predicts considerable covalency and ligand contributions with opposite signs relative to the dominating valence contribution.

The Mössbauer spectra in Figures 8A and 9 prove that the interpretation invoking the photolytic formation of a mixed-valent dinuclear species from **2** is correct. While it is very likely that the configuration of the cyclam ligand of the [(cyclam)-$Fe^{III}(N_3)$] fragment in the μ-nitrido-bridged complex is *cis* (only then a local $S = {}^5/_2$ spin state of the ferric ion can be attained), it is unclear what the configuration of the [(cyclam)$Fe^{IV}(N_3)$] fragment is in the product. In principle, both a *cis*- and a *trans*-configuration are compatible with a low-spin Fe^{IV} ($S = 1$) electron configuration. The latter would require a fast *cis* → *trans* isomerization step during the formation of the dinuclear product. This could happen during the formation of a [(cyclam)-$Fe^{V}(N)(N_3)$] intermediate as depicted in eq 4

$$cis\text{-}[(cyclam)Fe^{III}(N_3)_2]^+ \xrightarrow[-N_2]{h\cdot\nu} trans\text{-}[(cyclam)Fe^{V}(N)(N_3)]^+ \quad (4)$$

In summary, we propose that photolysis of **2** leads to a dinuclear μ-nitrido-bridged species containing a mixed-valent $[Fe^{III}(\mu\text{-}N)Fe^{IV}]^{4+}$ $S_t = {}^3/_2$ core. We propose either structure A or B shown in Scheme 1 for this species. Due to the fact that the Mössbauer parameters for the *trans*-[(cyclam)$Fe^{IV}(N_3)$] moiety in the photolysis products of **2** and **1a** are very similar, we favor structure A (see below).

The photolysis reaction of **1a** at −35 and 20 °C using the same reaction conditions as described above for **2** gives after ∼15 min of illumination a brown-yellow solution. Figure 6 shows the spectral changes observed during this period of illumination; the CT bands at 500, 350, 300, and 250 nm of **1a** lose intensity, whereas a new band at ∼400 nm appears. The final spectrum is very similar to that of the photolysis product of **2**. Upon prolonged illumination of this solution for 2 and 12 h a color change from brown-yellow to green and then to deep blue is observed. We have not characterized these products.

The X-band EPR spectrum at 10 K of a 15-min photolyzed solution of **1a** is shown in Figure 7B which is to be compared with the spectrum of the starting material shown in Figure 2.

(42) Oosterhuis, W. T.; Lang, G. *J. Chem. Phys.* **1973**, *58*, 4757−4765.
(43) Paulsen, H.; Müther, M.; Grodzicki, M.; Trautwein, A. X.; Bill, E. *Bull. Soc. Chim. Fr.* **1996**, *133*, 703−710.

Table 5. Mössbauer Parameter for Complexes Containing the $[Fe(\mu\text{-}N)Fe]^{4+}$ Core at 80 K

complex[h]	S_t	δ, mm s^{-1} [a]	ΔE_Q, mm s^{-1} [b]	Γ, mm s^{-1} [c]	%[d]	ref
$[\{LFe(Cl_4\text{-cat})\}_2(\mu\text{-}N)]$	$^3/_2$	0.52	1.67	0.77	45.6	14
		0.09	0.81	0.22	45.2	
$[\{LFe(nadiol)\}_2(\mu\text{-}N)]$	$^3/_2$	0.44	1.45	0.70	40.3	15
		0.07	0.85	0.38	41.3	
$[L(Ph_2acac)Fe(\mu\text{-}N)Fe(Cl_4\text{-cat})L]^+$	$^3/_2$	0.60	2.00	1.70	44	15
		0.04	1.13	0.31	44	
$[\{(cyclam)Fe(N_3)\}_2(\mu\text{-}N)]^{2+}$	$^3/_2$	0.47	1.89	0.71[e]	47	this work
		0.14	0.79	0.36	46	
		0.46	0.29	1.10	7[g]	
$[\{(tpp)Fe^{3.5}\}_2(\mu\text{-}N)]$	$^1/_2$	0.18	1.08	1.07		*f*
$[\{(pc)Fe^{3.5}\}_2(\mu\text{-}N)]$	$^1/_2$	0.06	1.76			10
$[(tpp)Fe^{3.5}(\mu\text{-}N)Fe^{3.5}(pc)]$	$^1/_2$	0.11	1.47			11
$[\{trans\text{-}(cyclam)(N_3)Fe\}_2(\mu\text{-}N)]^{2+}$	$^1/_2$	0.20	2.09	0.36[e]	40	this work
		0.11	0.97	0.67	42	
		0.54	0.65	0.36	18[g]	

[a] Isomer shift referenced vs α-Fe at 298 K. [b] Quadrupole splitting. [c] Line width at half-height. [d] Relative intensity of signal. [e] Doublet with asymmetric linewidths. [f] English, D. R.; Hendrickson, D. N.; Suslick, K. S. *Inorg. Chem.* **1988**, *22*, 367. [g] Impurity. [h] Ligand abbreviations: Cl_4-cat = tetrachlorocatecholate(2−), nadiol = naphthalene-2,3-diolate(2−), L = 1,4,7-trimethyl-1,4,7-triazacyclononane, acac = pentane-1,4-dionate(2−), Ph_2acac = 1,3-diphenylpropane-1,3-dionate(2−), tpp = tetraphenylporphinate(2−), pc = phthalocyaninate(2−).

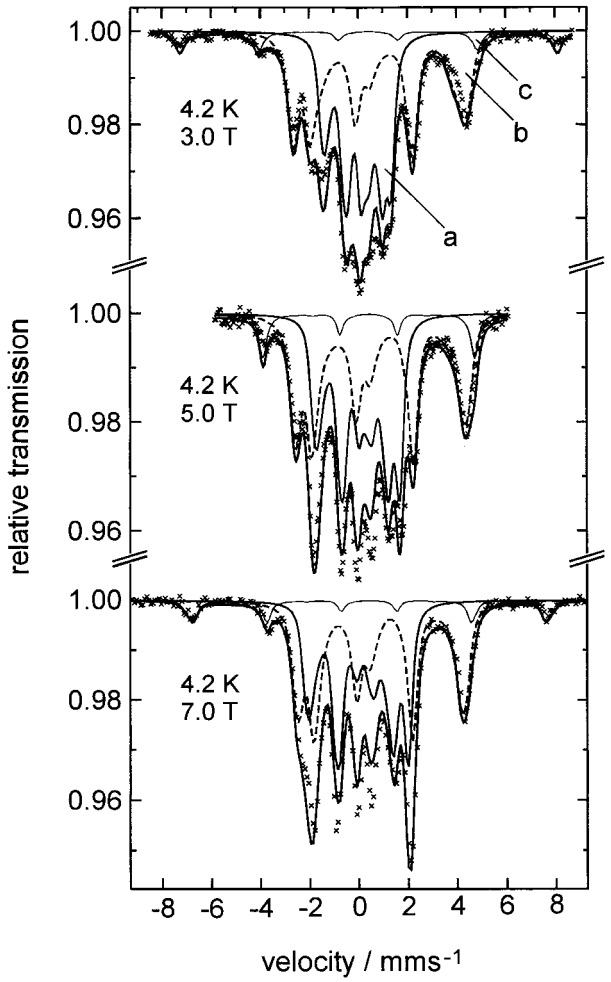

Figure 9. Magnetically perturbed Mössbauer spectra of **2** in CH_3CN after 60 min of photolysis at −35 °C. The sample is the same as that used for Figure 8A. The indicated subspectra are the result of spin-Hamiltonian simulations with $S_t = {}^3/_2$ for Fe^{IV} (a) and Fe^{III} (b), and $S = {}^5/_2$ for a 7% contribution of monomeric high-spin Fe^{III} (c), as described in the text.

Clearly, the rhombic signal of **1a** has changed into a new narrow $S = {}^1/_2$ signal with $g_1' = 2.04$, $g_2' = 2.06$, and $g_3' = 2.20$. Quantitation of this signal by double integration yields 0.44 spins/Fe. This spectrum is very similar to those reported for dinuclear, mixed-valent complexes containing the $[Fe(\mu\text{-}N)Fe]^{4+}$ core with an $S = {}^1/_2$ ground state as the data compiled in Table 4 show. A small difference is found, however, in the symmetry of the *g*-values. Whereas the porphyrin and phthalocyanin dimers show $g_\perp > g_{||}$, the photoproduct of **1a** has $g_{||} > g_\perp$.

Table 6. Spin Hamiltonian and Hyperfine Parameters of the Solution Photolysis Products Containing the $[Fe^{III}(\mu\text{-}N)Fe^{IV}]^{4+}$ Core at 4.2 K

	photolyzed **2**		photolyzed **1a**	
	Fe^{III}	Fe^{IV}	Fe^{III}	Fe^{IV}
S_t	$^3/_2$		$^1/_2$	
D, cm^{-1}	9(±3)			
E/D	0.02			
$\bar{g}$	(1.98, 1.989, 2.0)[a]		(2.04, 2.06, 2.20)[a]	
$A_x^{eff}/g_N\beta_N$, T	−18.90	+3.98	−4.74	+9.05
$A_y^{eff}/g_N\beta_N$, T	−20.22	+4.18	−12.97	+6.72
$A_z^{eff}/g_N\beta_N$, T	−31.79	+0.47	−32.76	+0.75
$A_{iso}^{eff}/g_N\beta_N$ [b]	−23.64	+2.88	−16.82	+5.51
$A_x/g_N\beta_N$ [c]	−13.50	−9.95	−2.8	−13.57
$A_y/g_N\beta_N$ [c]	−14.45	−10.45	−7.8	−10.07
$A_z/g_N\beta_N$ [c]	−22.70	−1.17	−19.7	−1.13
δ, mm s^{-1}	0.50	0.14	0.23	0.12
ΔE_Q, mm s^{-1}	−1.89	+0.88	−2.10	+0.98
η	0.03	0.74	0.85	0.4
Γ, mm s^{-1}	0.3	0.3	0.3	0.3

[a] Taken from (effective) EPR *g*-values. [b] Isotropic part; $^1/_3$Tr($\bar{\mathbf{A}}^{eff}$). [c] Intrinsic $\bar{\mathbf{A}}$ tensor components, derived from effective values by using eq 9 or 10, respectively.

The Mössbauer spectrum at 80 K of a 15-min photolyzed solution of a 35% ^{57}Fe-enriched sample of **1a** confirms the dimeric structure of the product; the spectrum is shown in Figure 8B. Lorentzian fits show the presence of two major quadrupole doublets a′ and b′ of practically equal intensities and an additional minor component c′. Since subspectrum a′ with $\delta = 0.11$ mm s^{-1}, $\Delta E_Q = 0.97$ mm s^{-1}, and 42% relative intensity is very similar to a of photolyzed **2** (Figure 8A), it is assigned to low-spin Fe^{IV} ($S = 1$). The parameters of species b′ ($\delta = 0.20$ mm s^{-1}, $\Delta E_Q = 2.09$ mm s^{-1}, 40% relative intensity) are only slightly different from those of **1a** starting material and could be well attributed to low-spin ferric iron. Magnetic Mössbauer measurements show, however, that this interpretation with respect to the spin state is not consistent with the magnetic hyperfine coupling scheme of a′ and b′ and the dimer spin $S_t = {}^1/_2$ (see below). Nevertheless, we can infer from these observations that the photolysis product of **1a** consists of a mixed-valent μ-nitrido dinuclear species containing now an $[Fe(\mu\text{-}N)Fe]^{4+}$ core with an $S_t = {}^1/_2$ ground state and *localized* Fe^{III}

Scheme 1. Proposed Structures for the (μ-Nitrido)diiron Photolysis Products

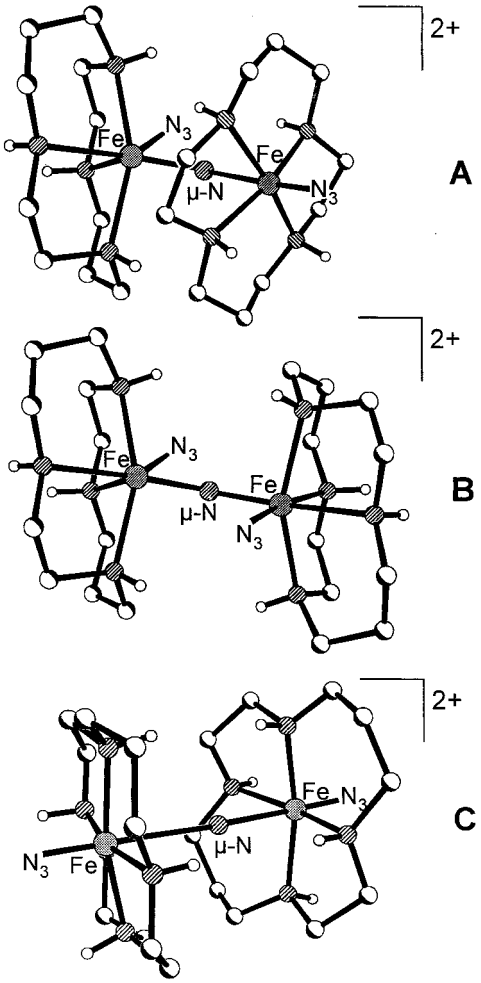

and Fe^{IV} valencies (class II).

$$2\ \mathbf{1a} \xrightarrow{h\cdot\nu} [\textit{trans}\text{-(cyclam)}_2\{Fe^{III}(\mu\text{-N})Fe^{IV}\}(N_3)_2]^{2+} + 2.5\ N_2 \quad (5a)$$

Thus we propose structure C for the photolysis product of **1a** (Scheme 1). This result contrasts considerably with the interpretation of the Mössbauer spectra of the nitrido-bridged diiron porphyrin and phthalocyanin complexes for which the iron sites were found to be indistinguishable even at 4.2 K, at least on the time scale of the ^{57}Fe nuclear lifetime and quadrupole precession time ($10^{-7}-10^{-8}$ s). Hence, *delocalized* valences have been proposed.[6,9-12] There is, however, a problem in this interpretation inasmuch as the dimer spin is not consistent with valence delocalization, unless the delocalization mechanism would be only a fast dynamic process (electron hopping) and not a quantum mechanically coherent superposition. For mixed-valent complexes with weakly interacting, bridged transition-metal pairs the coherent processes (double exchange) are spin-dependent and favor maximal spin multiplicity for the ground state, in contrast to the observation of energetically well isolated $S_t = {}^1/_2$ states. The *localized* valences in our complexes are, in this sense, consistent with the theoretical considerations.

The nature of the minority component in the Mössbauer spectrum of photolyzed **1a** (c′; 18% relative intensity) cannot be readily determined from the zero-field measurements. According to isomer shift $\delta = 0.54$ mm s^{-1} and quadrupole splitting $\Delta E_Q = 0.65$ mm s^{-1}, it could be either a high-spin ferric deterioration product ($S = {}^5/_2$) or a low-spin ferrous compound ($S = 0$). Since no high-spin signal was detected in the corresponding EPR spectra, the explanation that c′ might be Fe^{III} can be ruled out. Alternatively, the presence of $Fe^{III}(\mu$-oxo) dimers can also be excluded because these usually show much larger quadrupole splittings $|\Delta E_Q| > 1.0$ mm s^{-1}.[14,15,44,45] Magnetic Mössbauer measurements given below confirm that c′ is diamagnetic ($S = 0$). We assume therefore that c′ is a low-spin Fe^{II}(cyclam) complex which is formed during photolysis in addition to the $[Fe^{III}(\mu\text{-N})Fe^{IV}]^{4+}$ dimers. In accord with this interpretation the Mössbauer parameters of c′ closely resemble those of *trans*-$[(\text{cyclam})Fe^{II}(N_3)_2]$ (Figure 3A, bottom) and low-spin Fe^{II} porphyrinates ($\delta = 0.4-0.5$ mm s^{-1}, $\Delta E_Q = 0.6-1.4$ mm s^{-1}).[29] As the low-spin state in these systems is induced by strong ligand fields due to six-coordination, we propose that c′ is also a six-coordinate species. Presumably, it is generated by homolytic Fe−N_3 bond cleavage of **1a** and abstraction of $N_3^{\bullet}$, followed by binding of a CH_3CN solvent molelcule to accomplish the six-coordination of Fe^{II}.

$$\mathbf{1a} \xrightarrow{h\nu} \textit{trans}\text{-}[(\text{cyclam})Fe^{II}(N_3)(CH_3CN)] + N_3^{\bullet} \quad (5b)$$

This is the first experimental indication that formation of Fe^{II} is a relevant primary step in the photolyses of iron(III) azides.

Magnetic Mössbauer spectra were measured to probe the spin density distribution and the coupling scheme of the photolysis product of **1a**. Figure 10 shows spectra recorded with applied fields of 5 and 7 T at 4.2 and 80 K. The rather small overall splitting of less than 6 mm s^{-1} indicates weak internal fields due to the low spin expectation value and weak hyperfine coupling constants. At low temperatures (2.5−10 K) the spectra could be simulated in the limit of slow spin relaxation. Figure 10C shows that at 80 K this is only insufficiently possible. On the other hand, with applied field the limit of fast relaxation was also not fully reached at temperatures up to 180 K.

We could not detect any resolved contribution from the minority species c′ found in the zero-field measurement. Particularly, no high-spin Fe^{III} subspectrum was present like (c) in Figure 9. Also, the shoulders in the experimental spectra at about ±3 mm s^{-1} could not be attributed to a $S = {}^5/_2$ subspectrum even with unrealistically low $\bar{\mathbf{A}}$-values. Thus we had to conclude that c′ is not a paramagnetic species. Accordingly, a satisfactory fit to the measured spectra was possible by adopting $S = 0$ for c′ (with $\Delta E_Q > 0$, $\eta \cong 0$), as shown in Figure 10. This led us to conclude above that c′ is a ferrous low-spin species.

The magnetic spectra show a remarkable field dependence inasmuch as the outer prominent, more or less resolved lines at −2 mm s^{-1}, −0.8 mm s^{-1}, +1.3 mm s^{-1}, +1.8 mm s^{-1} *increase* their splitting with increasing applied field. This reveals a positive mean effective A value for the corresponding iron site which, thus, must be the site that is spin-oriented in an antiparallel fashion with respect to the total dimer spin. Surprisingly, it was not possible to simulate this important feature of the spectra with the parameters of the Fe^{III} site, subspectrum b′. Particularly the large quadrupole splitting of about 2.1 mm s^{-1} does not fit to the splitting pattern of the corresponding lines. In contrast, the pattern was easily reproduced with isomer shift and quadrupole splitting for the Fe^{IV} species, subspectrum a′. To this end we had to introduce positive

(44) Sage, J. T.; Xia, Y.-M.; Debrunner, P. G.; Keough, D. T.; Jersey, J. D.; Zerner, B. *J. Am. Chem. Soc.* **1989**, *111*, 7239.
(45) Rodriguez, J. H.; Ok, H.; Xia, Y.-M.; Debrunner, P. G.; Chaudhuri, P.; Wieghardt, K. *J. Am. Chem. Soc.* **1996**, *118*, 7542 and references therein.

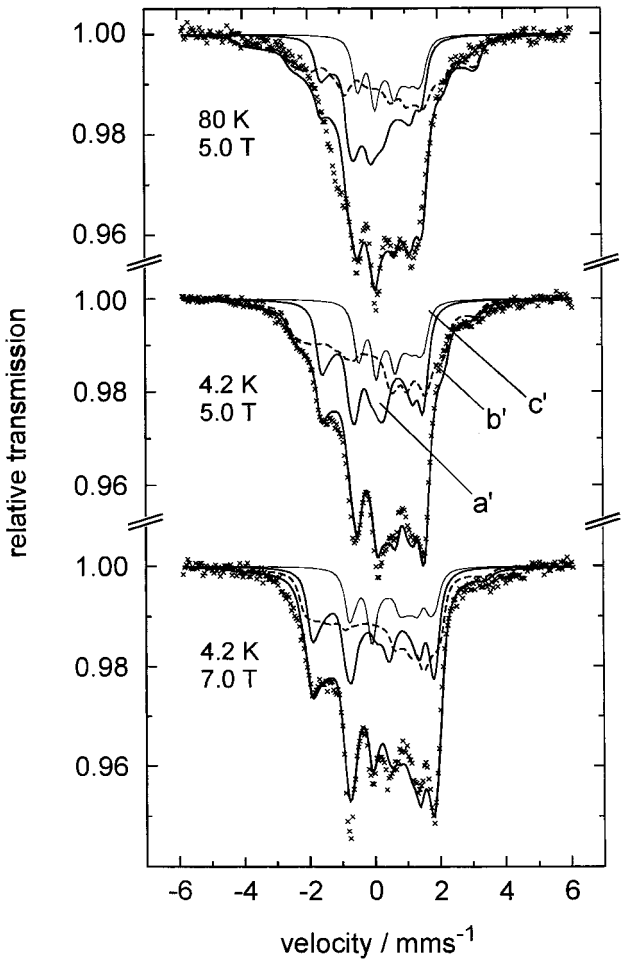

Figure 10. Magnetically perturbed Mössbauer spectra of **1a** in CH_3CN after 15 min of photolysis at 20 °C. The sample is the same as that used for Figure 8B. The indicated subspectra are the result of spin-Hamiltonian simulations with $S_t = {}^1/_2$ for Fe^{IV} a′ and Fe^{III} b′, and $S = 0$ for a 18% contribution of low-spin Fe^{II} c′, as described in the text.

$\bar{\mathbf{A}}$ values for a′. On the other hand, the broad, hardly resolved features of the spectra could be rather satisfactorily simulated with large quadrupole splitting of b′ and an anisotropic negative effective $\bar{\mathbf{A}}$ tensor. The parameters of the simulation are given in Table 6.

The positive effective $\bar{\mathbf{A}}$ tensor for Fe^{IV} and the negative $\bar{\mathbf{A}}$ tensor for Fe^{III} have the important implication that Fe^{IV} must have a *lower* local spin than Fe^{III}, i.e., Fe^{III} cannot be low-spin ($S_2 = {}^1/_2$). With the reasonable assumption based on the corresponding isomer shift and quadrupole splitting, that Fe^{IV} a′ is still low-spin ($S_1 = 1$) we have to conclude that Fe^{III} b′ is *intermediate-spin* ($S_2 = {}^3/_2$) in order to understand the cluster spin $S_t = {}^1/_2$ and the effective $\bar{\mathbf{A}}$ tensors of the subspectra a′ and b′ in the photolysis product of **1a**. When the effective $\bar{\mathbf{A}}$ tensor components of Fe^{IV} and Fe^{III} are converted to intrinsic values with the assumption that the respective local spins are $S_1 = 1$ (Fe^{IV}) and $S_2 = {}^3/_2$ (Fe^{III}) one obtains with spin projection factors according to eq 10: $\bar{\mathbf{A}}(Fe^{IV})/g_N\beta_N = (-13.57, -10.07, -1.13)$ T and $\bar{\mathbf{A}}(Fe^{III})/g_N\beta_N = (-2.8, -7.8, -19.7)$ T.

The $\bar{\mathbf{A}}$-values for Fe^{IV} compare very well with those of Fe^{IV} in the photolysis product of the *cis*-isomer **2**, according to what was found before for isomer shift and quadrupole splitting (see Table 6). This confirms again that both the photolysis products of **1a** and of **2** possess an $[Fe(\mu\text{-}N)Fe]^{4+}$ core with localized valences and with apparently very similar coordination at the Fe^{IV} ion, namely *trans*-[(cyclam)Fe^{IV}].

Iron(III) intermediate-spin complexes on the other hand are relatively rare. A compilation of data for porphyrinates is found in refs 29 and 46; other examples were also intensively studied, like dithiocarbamates and salen complexes.[47−49] The intermediate spin state in these compounds is related to five-coordination (square-pyramidal geometry) with strong equatorial ligands or with six-coordination and weak axial ligands. Some iron nitrosyl complexes of the type $\{FeNO\}^7$ also show spin $S = {}^3/_2$. However, this state was recently described for a synthetic model on the basis of X-ray absorption measurements and MO calculations as a spin-coupled system composed of formally Fe^{III} ($S = {}^5/_2$) and NO^- ($S = 1$).[50]

Usually square planar geometry was taken as the starting point for theoretical descriptions of ferric $S = {}^3/_2$ systems, with the assumption that the $d_{x^2-y^2}$ orbital is strongly destabilized and too high in energy to be populated. The corresponding formal $(d_{xy})^2(d_{xz})^1(d_{yz})^1(d_{z^2})^1$ configuration is consistent with most experiments. Maltempo[30] pointed out that to some degree the quartet state $^4A_2$ is mixed into the $^6A_1$ ground state of all ferric high-spin porphyrins, and this accounts for, for instance the zero-field splitting. The Maltempo model describes the magnetic properties of the intermediate spin systems reasonably well on the basis of spin-mixing between $^4A_2$ and $^6A_1$ states. The $\bar{\mathbf{A}}$ tensors, particularly those of the intermediate-spin porphyrinates show large anisotropies due to strong spin−dipolar contributions that are correctly predicted in this picture (at least concerning the symmetry). For the $(d_{xy})^2(d_{xz})^1(d_{yz})^1(d_{z^2})^1$ ground-state, strong dipolar fields are found to oppose the isotropic Fermi contact contribution in the *z*-direction and to enforce it in the *x*/*y*-plane. The "inverse" symmetry, however, is found for $\bar{\mathbf{A}}(Fe^{III})$ in the photoproduct of **1a** (Table 6): A_z is large and negative, and the *x*- and *y*-components are small. We cannot probe other magnetic properties of the Fe^{III} site in the dimeric photolysis product of **1a** independently since spin coupling is apparently the dominant interaction. It appears, however, that the $\bar{\mathbf{A}}$ tensor anisotropy is not consistent with the usual ground-state configuration $(d_{xy})^2(d_{xz})^1(d_{yz})^1(d_{z^2})^1$ of Fe^{III} ($S = {}^3/_2$).

Also the experimental efg contradicts the usual electronic structure for intermediate-spin complexes. A hypothetical pure $(d_{xy})^2(d_{xz})^1(d_{yz})^1(d_{z^2})^1$ electronic ground state leads to a vanishing valence contribution to the efg. Nevertheless, the investigated intermediate spin complexes show typically large positive quadrupole splittings of more than 2 mm s^{-1} and a small asymmetry parameter. The positive sign of V_{zz} implies excessive negative charge in the equatorial plane which must arise from strong covalency effects. The iron(III) site in the photolysis product of **1a**, however, shows a large negative quadrupole splitting, also of about 2 mm s^{-1}, but with a large asymmetry parameter. Although the negative sign is not very significant in this case (since the asymmetry parameter η is close to 1, the

(46) (a) Scheidt, W. R.; Osvath, S. R.; Lee, Y. J.; Reed, C. A.; Shaevitz, B.; Gupta, G. P. *Inorg. Chem.* **1989**, *28*, 1591−1595. (b) Gupta, G. P.; Lang, G.; Reed, C. A.; Shelly, K.; Scheidt, W. R. *J. Chem. Phys.* **1987**, *86*, 5288−5293.

(47) (a)Niarchos, D.; Kostikas, A.; Simopoulos, A.; Coucouvanis, D.; Piltingsrud, D.; Coffman, R. E. *J. Chem. Phys.* **1978**, *69*, 4411−4418. (b) Ganguli, P.; Marathe, V. R.; Mitra, S. *Inorg. Chem.* **1975**, *14*, 970−973. (c) Ganguli, P.; Hasselbach, K. M. *Z. Naturforsch.* **1979**, *34a*, 1500−1506. (d) Wells, F. V.; McCann, S. W.; Wickman, H. H.; Kessel, S. L.; Hendrickson, D. N.; Feltham, R. D. *Inorg. Chem.* **1982**, *21*, 2306−2311.

(48) Koch, W. O.; Schünemann, V.; Gerdan, M.; Trautwein, A. X.; Krüger, H.-J. *Chem.−Eur. J.* **1998**, *4*, 686−691.

(49) (a) Kuang, X.-Y.; Morgenstern, I.; Rodriguez, M.-C. *Phys. Rev. B* **1993**, *48*, 6676−6679. (b) Kuang, X.-Y.; Morgenstern-Badarau, I. *Phys. Status Solidi B* **1995**, *191*, 395−400.

(50) Brown, C. A.; Pavlosky, M. A.; Westre, T. E.; Zhang, Y.; Hedman, B.; Hodgson, K. O.; Solomon, E. I. *J. Am. Chem. Soc.* **1995**, *117*, 715−732.

limit at which V_{yy} has the same magnitude as V_{zz} but opposite sign), the asymmetry might owe its origin to contributions of valence and covalency.

The isomer shifts of the known intermediate-spin complexes are in the range 0.3−0.4 mm s^{-1} [29,46−48] which is intermediate between typical values for low-spin and high-spin complexes. For Fe^{III} in the photolysis product of **1a** the isomer shift is somewhat below the value of the starting complex **1a**. This points toward an increased covalency instead of a decreased interaction, as would be expected if weakening of the axial bonds in the photoproduct had induced the intermediate spin state. Taking together the spectroscopic observations of the unusually low isomer shift, the unusual efg and the "inverted" symmetry of the $\bar{\mathbf{A}}$ tensor, we are tempted to suggest that a new *strong* axial bond, namely, the nitrido-iron bond, leads to the spin quartet ground state of Fe^{III} in the photolysis product of **1a**. One could envisage basically linear geometry as the starting point for the understanding of this species. Then the d_z^2 orbital would be too strongly destabilized to be populated in the spin quartet state. Further experimental and theoretical investigations concerning the influence of the μ-nitrido bridge will address these questions.

Photolyses at 4 and 77 K. The above photolyses have been carried out in the liquid phase where rapid bimolecular dimerization processes yielding complexes containing the [Fe(μ-N)-Fe]$^{4+}$ cores ($S_t = {}^3/_2$ or ${}^1/_2$) prevent the build-up of the putative mononuclear intermediate *trans*-[N═Fe^V(cyclam)(N_3)]$^+$. Therefore, we have carried out a series of photolysis experiments in *frozen* acetonitrile solution of **1a** and **2**, where the immobilized reactants should not be able to undergo subsequent bimolecular processes and, thus, allow the spectroscopic detection of primary intermediates. In this program the *trans*-[Fe^{III}(cyclam)$(N_3)_2$]$^+$ complex **1a** in contrast to **2** has the advantage that its narrow $S = {}^1/_2$ EPR signal should not overlap with the low-field resonances of the $S = {}^3/_2$ spectrum that is anticipated for the target Fe^V═N intermediate. Therefore, we have investigated the low-temperature photolysis products of **1a** first.

Several techniques were used to prepare EPR and Mössbauer samples, including in situ photolysis at 4.2 K, in the respective spectrometer cryostats. The best results with high yields of the primary products were obtained by illuminating finely ground, frozen solutions in liquid nitrogen (method II, Experimental Section). A zero-field Mössbauer spectrum of such a preparation after 75 min of illumination at 419 nm is shown in Figure 11A. High conversion of the starting compound **1a** (typically 80%) and formation of a distinct main product are recognized from the strong attenuation of the original spectrum (Figure 3A, top) and the appearance of a dominating new quadrupole doublet with a significantly lower isomer shift than **1a** (subspectrum **OX**). Additional lines at high velocities around 2−3 mm s^{-1} indicate the presence of further, somewhat less abundant iron species with large isomer shifts and large quadrupole splittings, which are characteristic of Fe^{II} ions (subspectra **FeII(1)**, **FeII(2)**, **FeII(3)**, see Scheme 2). The deconvolution of the experimental spectrum into these subspectra is the result of least-squares fits with Lorentzian doublets which were performed simultaneously for up to six experimental spectra from preparations with different light exposure times, wavelengths, and sample preparation techniques including in situ photolysis at 4.2 K (Figure 11C). The respective subspectra were forced to be consistent for the different experimental conditions by using the same Mössbauer parameters for all experimental spectra, except for the line widths and intensities of the doublets which were treated as independent variables for each experimental spectrum. The fit results are given in Table 7 for three different photolytic preparations.

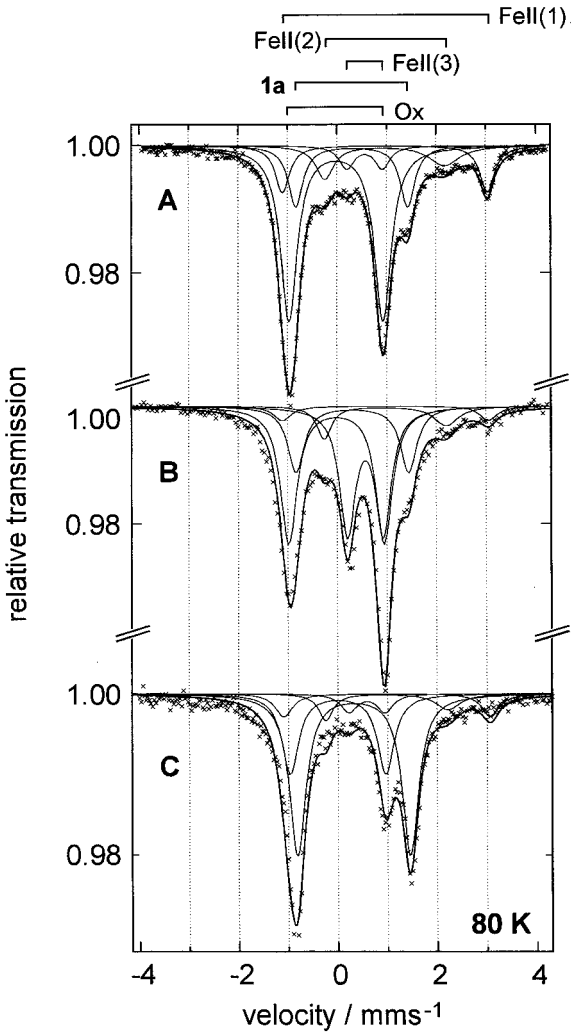

Figure 11. Zero-field Mössbauer spectra (80 K) of ^{57}Fe-enriched (35%) **1a** in CH_3CN (1.7 mM); (A) after 70 min of irradiation at 419 nm at liquid-nitrogen temperature (method II); (B) after subsequent annealing of this sample at 160 K for 15 min; (C) **1a** in CH_3CN (1.7 mM) after irradiation with an HBO lamp at 4.2 K in the Mössbauer cryostat (method I). Virtually the same spectrum was obtained at 4.2 K immediately after irradiation at 4.2 K.

The comparatively high yield of the new species **OX** obtained by illuminations at 77 K (method II) as well as at 4.2 K (method I) shows that **OX** is a primary photolysis product of **1a**. Repeated measurements on samples stored in liquid nitrogen showed that this product is stable at 77 K for weeks. After annealing the sample at 160 K for 15 min it was found that the intensity of the **OX** signal dropped by only ∼10% (Table 7). To our surprise however, the annealing experiment revealed a marked instability of one of the Fe^{II} species formed by photolysis. Figure 11B shows that after annealing **FeII(1)** essentially disappeared, whereas **FeII(2)** remained unchanged and the relative intensity of the **FeII(3)** signal increased from 6 to 27%. This shows that at least **FeII(1)** is also a primary photolysis product of **1a**. The Mössbauer parameters of **FeII(1)** ($\delta = 0.95$ mm s^{-1}, $\Delta E_Q = 4.13$ mm s^{-1}) closely resemble those of high-spin, five-coordinate Fe^{II} porphyrins with ionic axial ligands such as $CH_3CO_2^-$ ($\delta = 1.03-1.05$ mm s^{-1}, $\Delta E_Q = 4.01-4.25$ mm s^{-1}).[51] Therefore, we assign **FeII(1)** to five-coordinate [Fe^{II}(cyclam)(N_3)]$^+$ ($S = 2$) with cyclam in its "planar" *trans*-configuration (Scheme 2). We propose that

Scheme 2. Preparation and Labels of Ferrous Complexes

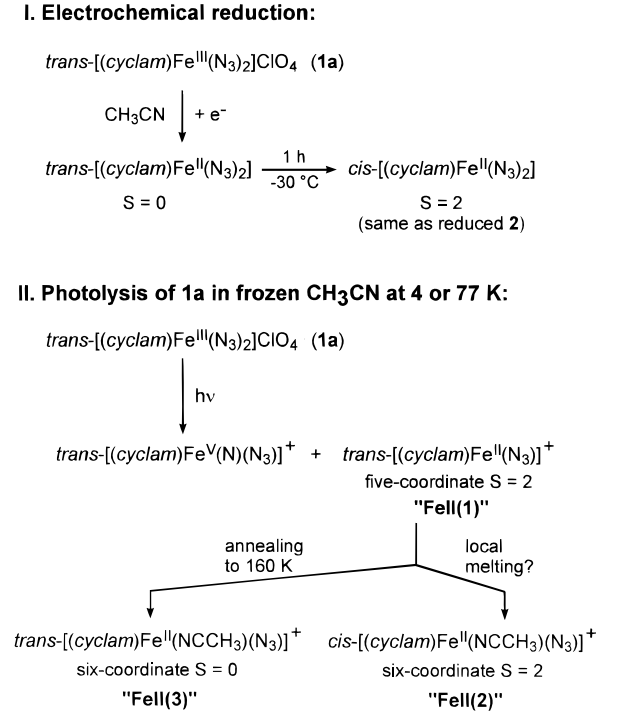

FeII(1) is formed from **1a** via homolytic $Fe^{III}-N_3$ bond cleavage where the *trans*-configuration of cyclam is trapped in the frozen matrix.

The Mössbauer parameters of low-spin, six-coordinate *trans*-[Fe^{II}(cyclam)$(N_3)_2$] given above (Figure 3A, bottom, I) are virtually identical to those of **FeII(3)** in the photolyzed samples. Therefore, the parameters of **FeII(3)** were fixed to those values in the fits in order to reduce the number of variables. Thus, we assign **FeII(3)** to low-spin, six-coordinate *trans*-[Fe^{II}(cyclam)(N_3)X] where X might be a solvent molecule. It is then tempting to assume that during annealing, **FeII(1)** is converted to **FeII(3)** by coordination of a neighboring CH_3CN solvent molecule. Finally, the Mössbauer parameters of **FeII(2)** are quite similar to those of electrochemically generated *cis*-[Fe^{II}(cyclam)$(N_3)_2$] (Figure 3B, subspectrum II) which in liquid solution has the most stable configuration. During photolysis in frozen solution the corresponding six-coordinate *cis*-species with a coordinated solvent molecule might have been formed from the *trans*-complex **1a** by local melting immediately after photon absorption. During annealing at 160 K, however, its abundance remained stable because local melting does not occur.

If no care was taken to avoid contamination of the sample with water and/or oxygen before low-temperature photolysis, the photolyzed samples showed a much lower amount of Fe^{II} species than that obtained with oxygen-free samples. In particular, **FeII(1)** was usually completely absent. Instead, another broad subspectrum appeared in the Mössbauer spectra with a high isomer shift $\delta \sim 0.5$ mm s^{-1} (indicative of Fe^{III} high-spin) and large quadrupole splitting $\Delta E_Q \approx 1.9$ mm s^{-1}. This spectrum might represent an unknown decomposition (oxidation or hydrolysis?) product; it is quite similar to complexes containing an $[Fe^{III}-O-Fe^{III}]^{4+}$ moiety with antiferromagnetically coupled high-spin ferric ions.[14,15,44,45] We have independently synthesized such a species, namely [{*cis*-(cyclam)Fe^{III}}$_2$(μ-O)(μ-CO_3)]$(ClO_4)_2 \cdot 3H_2O$ the details of which will be reported elsewhere. This complex displays a Mössbauer spectrum at 80 K, consisting of a single quadrupole doublet with parameters $\delta = 0.47$ mm s^{-1}, $\Delta E_Q = 1.32$ mm s^{-1}.

Over-photolyzation of (dry or moist) samples by prolonged or more intense illumination especially with wavelengths <300 nm also leads to another new, very broad Mössbauer subspectrum with Fe^{III} (low-spin) character ($\delta = 0.3$ mm s^{-1}, $\Delta E_Q = 2.2$ mm s^{-1}). This is apparently a deterioration product, the formation of which limited also the formation of the target compound in higher yields during in situ illumination of thin sample layers at 4.2 K or in EPR tubes (method I).

Low-temperature photolyses at 77 and 4.2 K of *cis*-[Fe^{III}-(cyclam)$(N_3)_2$] (**2**) yielded only small amounts of a product in <5% yield which displayed a spectrum (not shown) which is comparable to that of **OX**. The major intensity of the product Mössbauer spectra was found for a subspectrum with $\delta = 1.06$ mm s^{-1} and $\Delta E_Q = 2.75$ mm s^{-1} which is close to that of **FeII(2)** which we attributed to a six-coordinate ferrous species. This means that under the present low-temperature conditions homolytic cleavage with concomitant binding of a solvent molecule dominates. Therefore, we did not investigate the photolysis of **2** in further detail.

X-band EPR spectra of the photolysis products of **1a** were recorded on aliquots of the Mössbauer preparations (method II). The EPR spectrum depicted in Figure 12 was recorded by using the same sample as was prepared for Mössbauer spectroscopy (Figure 11A). The original signal of low-spin **1a** (Figure 2) drastically lost intensity, and new signals around $g' = 4$ and 2 are observed. The spectrum shows strong line broadening, probably due to the presence of trace amounts of O_2;[52] overall, however, the features are characteristic of a spin quartet with axial symmetry, $E/D \approx 0$, and moderately large zero-field splitting, $D > h\nu$ (0.3 cm^{-1}).[39,53] A corresponding spin-Hamiltonian simulation with parameters taken from the Mössbauer analysis (see below) is shown as solid line in Figure 12B. According to this simulation, the main intensity of the spectrum at $g \approx 4$ originates essentially from "$(-1/2 \rightarrow +1/2)$" transitions for **B** field orientations close to the *xy*-plane. Level schemes as depicted in the inset of Figure 12 show, however, that also inter-doublet transitions and "$(-3/2 \rightarrow +3/2)$" transitions occur due to weak ZFS with $|D| = 0.38$ cm^{-1}, $E/D = 0.094$. In the powder summation these transitions give rise to a broad distribution of resonance absorptions. In the simulation large angular-dependent Gaussian line-widths ($\bar{W} = (60, 60, 120)$ mT) were used to match the broad experimental pattern. Since the Mössbauer spectra above showed that the other photolysis products of **1a** are EPR-silent ferrous compounds, one can infer that **OX** is the spin-quartet species observed in the EPR spectra.

Interestingly, the broad axial EPR spectrum of **OX** in Figure 12 is very similar to those reported for isoelectronic (porphyrin)-Mn^{IV}=O complexes.[17,54-56] The same broad axial signal at $g \approx 4$ with a trough at $g < 2$ has been observed for this Mn^{IV}=O

(51) Bominaar, E. L.; Ding, X.-Q.; Gismelseed, A.; Bill, E.; Winkler, H.; Trautwein, A. X.; Nasri, H.; Fischer, J.; Weiss, R. *Inorg. Chem.* **1992**, *31*, 1845.

(52) Freshly prepared EPR samples showed obscure signals in a broad field range, which changed drastically to what is shown in Figure 12 when the cold sample tube was evacuated for 20 min without warming above 77 K. This process is reversible; the initial shape of the spectrum before evacuation can be restored by exposure of the sample to dry (liquid) air. We assume that during packing of the frozen solution powder at 77 K into the EPR tube, triplet O_2 condensed into the material and then physically interacted with the paramagnetic iron species due to (dipolar) spin−spin interaction. At least in the relatively weak magnetic fields used for X-band EPR this can lead to severe spectral distortions.

(53) Mabbs, F. E.; Collison, D. *Electron Paramagnetic Resonance of d Transition Metal Compounds*; Elsevier: Amsterdam, London, New York, Tokyo, 1992.

(54) Groves, J. T.; Stern, M. K. *J. Am. Chem. Soc.* **1987**, *109*, 3812.

Table 7. Mössbauer Parameter of the Low-temperature Photolysis Products of **1a** Measured at 80 K[h]

				relative intensities, %		
subspectrum	δ, mm s^{-1}	ΔE_Q, mm s^{-1}	Γ, mm s^{-1}	method II[a]	annealed[b]	method I[c]
1a[d]	0.28	2.26	0.35	17	16	48
OX	−0.04	1.90	0.40	54	44	26
FeII(1)	0.95	4.13	0.35	12	3	7
FeII(2)	0.95	2.42	0.73[f]	11	10	10
FeII(3)[e]	0.55	0.72	0.35	6	27	8
				54/29 ratio **OX**/∑FeII[g]	44/40	26/25

[a] Photolyzed at 77 K for 70 min at 419 nm (method II); corresponding spectrum in Figure 11A. [b] Same sample as described in a), annealed at 160 K for 15 min, corresponding spectrum in Figure 11B. [c] Photolyzed at 4.2 K in the Mössbauer cryostat for 30 min with OSRAM HBO lamp (method I); corresponding spectrum in Figure 11C, practically the identical result was obtained in a zero-field measurement at 4.2 K. [d] δ, ΔE_Q fixed to values of pure starting complex **1a** (Table 2). [e] δ, ΔE_Q fixed to values of *trans*-[(cyclam)Fe^{II}(N$_3$)$_2$] (Table 2). [f] Average value; asymmetric line widths were allowed; the high-energy line was 60% broader than the low-energy line. [g] Ratio of relative intensities of **OX** vs **FeII(1)** + **FeII(2)** + **FeII(3)**. [h] Typical errors of δ and ΔE_Q are ±0.02 mm s^{-1}.

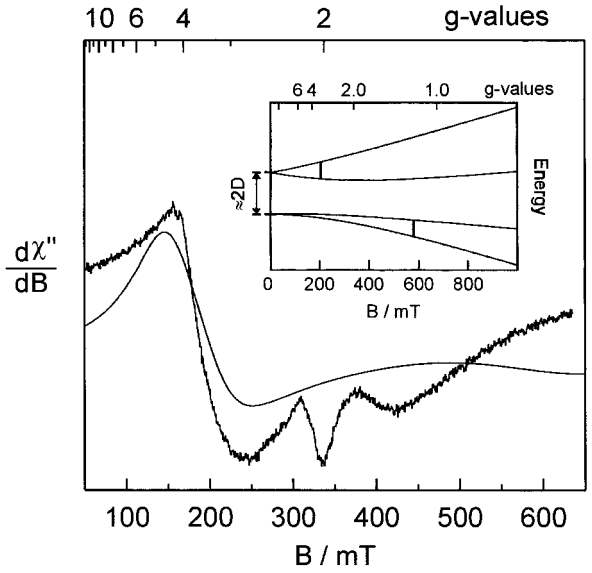

Figure 12. X-band EPR spectra (10 K) of **1a** in CH_3CN (1.7 mM) after low-temperature photolysis (method II). The sample was an aliquot of the Mössbauer sample used for the spectrum in Figure 11A. Before measurement it was evacuated for 20 min at 77 K. Experimental conditions: microwave frequency 9.451 GHz, microwave power 200 μW, modulation 1.25 mT and 100 kHz. The solid line is a spin-Hamiltonian simulation ($S = {}^3/_2$) with parameters as given in Table 8. The inset shows the energy levels of an $S = {}^3/_2$ multiplet according to eq 7 for the same zero-field parameters as a function of applied field in *x*-direction. The vertical lines indicate EPR transitions at 9.451 GHz.

species. Even the zero-field splitting $|D| = 1.3 \pm 0.3$ cm^{-1} which was inferred from comparisons with other mononuclear Mn^{IV} compounds[57] is similar to the value for the Fe^{V}═N species. Very similar spectra have also been published for (porphyrin)-Mn^{IV}(X)$_2$ complexes with X = N_3, NCO, and OCH_3 for which $|D| > 0.6$ cm^{-1} was estimated.[58] Slightly lower *D* values in the range 0.145−0.245 cm^{-1} are reported for isoelectronic (porphyrin)Cr^{III}(Cl)(X) complexes, where X represents one of a series of neutral ligands.[59]

In the 77 K preparations we did not detect significant contributions from azide radicals, $N_3^{\bullet}$, which should form in the same amount as Fe^{II} when Fe^{III}−azide bonds are homolytically cleaved. Only in in situ photolyses at 4.2 K the corresponding narrow free radical EPR signal at $g \approx 2.0$ is observed. The signal disappeared completely at liquid nitrogen temperatures. We assume that $N_3^{\bullet}$ radicals can diffuse rapidly and decompose to give N_2 even in the frozen matrix.

Magnetically perturbed Mössbauer spectra were measured to establish independently the spin state and the magnetic properties of the photolysis product **OX**. An annealed sample was selected for these measurements because it has a relatively low high-spin Fe^{II} content which does not contribute a subspectrum with unknown paramagnetic behavior. Spectra recorded with 3−7 T applied field at different temperatures are shown in Figure 13 together with simulations for **OX** and **FeII(3)**. The magnetic pattern of the latter (27%) was straightforwardly calculated because for the low-spin iron ($S = 0$) only the sign of V_{zz}, which is the main component of the electric field gradient (efg), and the asymmetry parameter η of the efg are unknown. The 16% spectral contribution of nonphotolyzed starting material **1a** was subtracted from the experimental data by using parameters obtained independently from measurements of pure **1a**. The weak (10%) contamination of **FeII(2)** ($S = 2$) was neglected in the spin-Hamiltonian analyses.

Since the X-band EPR spectra of **OX** showed perturbations from spin−spin interaction with molecular O_2,[52] we refrained from analyses of magnetic Mössbauer spectra with applied fields <3 T. One can reasonably expect that in stronger fields the dipolar spin interactions, which for intermolecular couplings usually are of the order 10^{-1} cm^{-1} or less, can be neglected because the spins are decoupled by the Zeeman effect (2.1 T × $\mu_B = 1$ cm^{-1}), and hence, the paramagnetic properties of **OX** can be observed.

The magnetic Mössbauer spectra of **OX** depicted in Figure 13 A−D show a broad pattern with several resolved features that reflect the effect of competing nuclear quadrupole and Zeeman interactions. The magnetic interaction is determined by the magnitude of the effective field $\mathbf{B}^{eff} = \mathbf{B} - \mathbf{B}^{int}$, where $\mathbf{B}^{int} = \bar{\mathbf{A}}\langle\mathbf{S}\rangle/g_N\beta_N$ is the internal field. The overall splitting of about 5 mm s^{-1} for the most prominent features of **OX** implies a relatively small internal field of 15 T; outer shoulders in the spectra, however, indicate also the presence of molecular orientations in the powder sample with larger fields. Details of the spectral pattern depend on the magnitude of the applied field at 1.8 K, whereas the total splitting is less field-dependent. The broad lines are characteristic of angular distributions of the internal field with respect to the efg principal axes. Temperature elevation at 3 T (Figure 13D) induces new components in the spectrum with larger splitting than those of the ground state. One can conclude from these qualitative observations that (i)

(55) Czernuszewicz, R. S.; Su, Y. O.; Stern, M. K.; Macor, K. A.; Kim, D.; Groves, J. T.; Spiro, T. G. *J. Am. Chem. Soc.* **1988**, *110*, 4158.
(56) Smegal, J. A.; Hill, C. L. *J. Am. Chem. Soc.* **1983**, *105*, 3515.
(57) Richens, D. T.; Sawyer, D. T. *J. Am. Chem. Soc.* **1979**, *101*, 3681.
(58) Camenzind, M. J.; Hollander, F. J.; Hill, C. L. *Inorg. Chem.* **1983**, *22*, 3776.
(59) Sommerville, D. A.; Jones, R. D.; Hoffman, B. M.; Basolo, F. *J. Am. Chem. Soc.* **1977**, *99*, 8195.

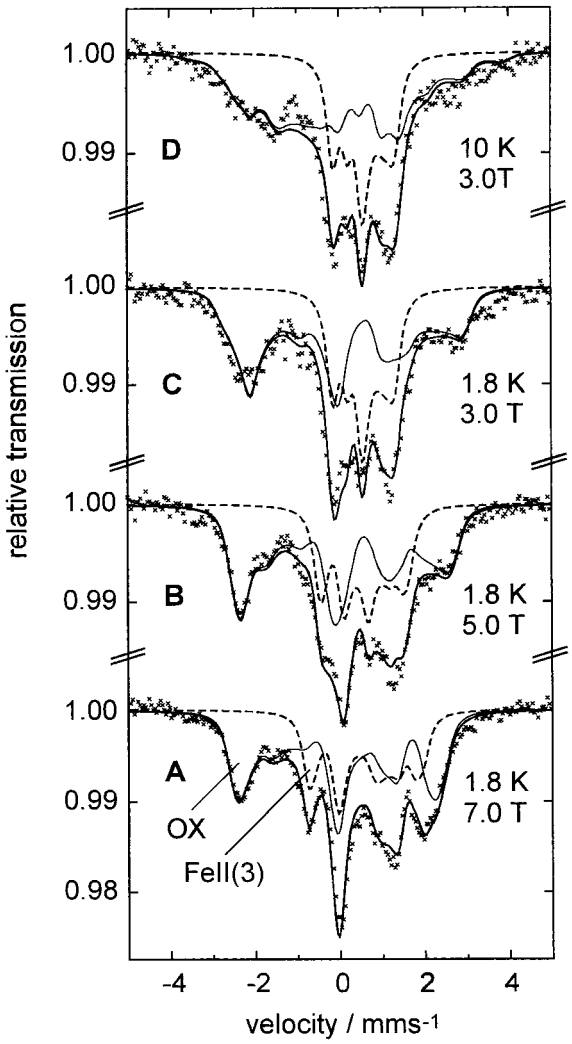

Figure 13. Magnetically perturbed Mössbauer spectra of irradiated **1a** (method II) obtained at liquid helium temperatures with the indicated perpendicular applied fields. The sample was the same as that used for Figure 11B. The contributions of residual starting material **1a** (16% relative intensity) are subtracted from the experimental data. The indicated subspectra **FeII(3)** and **OX** are spin-Hamiltonian simulations for $S = 0$ and $S = {}^3/_2$, respectively, as described in the text.

the isotropic part of $\mathbf{B}^{int}$ is relatively weak (with respect to $\mathbf{B}^{int} = 55$ T for Fe^{III} high-spin for example) due to either a small spin expectation value $<\mathbf{S}>$ or to a small isotropic part of $\boldsymbol{A}$; (ii) since the internal field appears to follow largely the direction of the applied field, the magnetic anisotropy of the electronic ground state is small or the ZFS is weak; (iii) the internal fields are stationary on the Mössbauer time scale.

These considerations for **OX** were further substantiated by computer simulations based on eqs 7 and 8, and the result is shown as solid lines in Figure 13. Isomer shift and quadrupole splitting were fixed in the simulations to the values from zero-field measurements at 4.2 K, the electronic *g*-values were fixed to 2.0, and the efg and $\bar{\mathbf{A}}$ tensor were kept collinear to the principal axes of the ZFS. For the low-spin ferrous contribution, **FeII(3)**, a diamagnetic spectrum was generated for which only the asymmetry parameter η and the sign of ΔE_Q were variables. The subspectra **OX** and **FeII(3)** were superimposed with relative weights of 62 and 38%, according to the ratio of their relative intensities of 44 and 27% in the original zero-field spectrum of the annealed sample. A genetic algorithm[60] was used for a systematic search in the parameter space with simultaneous least-squares optimization for the entire data set of six spectra. The result was refined with a downhill simplex procedure.[61] The final parameter set for **OX** is given in Table 8.

Table 8. Spin-Hamiltonian and Hyperfine Parameters of the Low-Temperature Photolysis Product of **1a** *trans*-$[Fe^V(N)(cyclam)(N_3)]^+$ (**OX**) ($S = {}^3/_2$)

D, cm^{-1}	-0.37 ± 0.15
E/D	0.095 ± 0.05
$\underline{g}$[a]	2.0
$\bar{\mathbf{A}}/g_N\beta_N$, T	$(-13.3, -10.6, 2.5)$ (± 0.2)
δ, mm s^{-1} [b]	-0.04 ± 0.01
ΔE_Q, mm s^{-1} [b]	-1.90 ± 0.02
η	0.6 ± 0.2

[a] Fixed to an isotropic value. [b] Taken from zero-field measurements at 4.2 K.

According to the qualitative observations, the ZFS parameter D turned out to be relatively small (-0.38 cm^{-1}) in conjunction with low rhombicity $E/D = 0.095$. The negative sign of D, however, is essential for the simulations in order to reproduce the field dependence at 1.8 K. At 7 T, the strongest field used in this study, the ZFS is dominated by the electronic Zeeman interaction which means that the m_s levels are in the order ($-{}^3/_2 \cdots +{}^3/_2$) with exclusive population of the ($m_s = -{}^3/_2$) ground state at 1.8 K. The spin expectation value $<\mathbf{S}>$ then is oriented essentially parallel along the applied field, irrespective of the field orientation in the molecular frame. The powder spectrum is therefore sensitive to the entire $\bar{\mathbf{A}}$ tensor. As the applied field decreases, excited m_s states are increasingly mixed into the ground level, and the internal field due to the increasing influence of ZFS tends to point along the molecular *z*-direction, owing to the negative D parameter with the low-lying $m_s = \pm {}^3/_2$ Kramers doublet in weak field. The extent of level mixing depends on the magnitude of the ZFS and, thus, can be used to determine the ZFS parameters. Increasing the temperature at moderate or weak field affects the population of excited levels and, hence, probes also the ZFS.

The fit of the field dependence of the spectra from **OX** requires a very anisotropic $\bar{\mathbf{A}}$ tensor with positive A_z component. The isotropic contribution ${}^1/_3\mathrm{Tr}(\bar{\mathbf{A}})/g_N\beta_N$ is only -7.1 T. The asymmetric and broad absorptions in the spectrum arise from the anisotropic internal field strength due to anisotropic $\bar{\mathbf{A}}$ in conjunction with the angular distribution of field orientations in the powder sample. The most prominent lines owe their origin to the relatively large solid-angle contributions where the angular components of the anisotropic $\bar{\mathbf{A}}$ tensor are close to zero (because of the presence of negative and positive main *A*-components). Significantly, a corresponding spin-Hamiltonian analysis of the magnetic Mössbauer spectra of **OX** with the assumption of low-spin $S = {}^1/_2$ ground state did not give satisfactory fits to the field dependence of the spectra. Hence, the spin state $S = {}^3/_2$ for **OX** is unambiguously established by Mössbauer spectroscopy.

The EPR and Mössbauer data described above clearly show that photolysis with UV light of *trans*-$[(cyclam)Fe^{III}(N_3)_2](ClO_4)$ produces an intermediate with an $S = {}^3/_2$ ground state and unique Mössbauer parameters with an isomer shift of -0.04 mm s^{-1} at 80 K and a large quadrupole splitting of $\sim$1.9 mm s^{-1}. We propose the following structure for this species: a six-coordinate cation *trans*-$[N{=}Fe^V(cyclam)(N_3)]^+$ (Scheme 3).

It is quite remarkable that the isomer shifts of (i) low-spin **1a** (d^5), (ii) its one-electron reduced, low-spin ferrous form (d^6),

(60) Goldberg, D. E. *Genetic Algorithms in Search, Optimization, and Machine Learning*; Addison-Wesley: Reading. MA, 1989.
(61) Press: W. H.; Flannery, B. P.; Teukolsky, S. A.; Vettering, W. T. *Numerical Recipes*; Cambridge Unversity Press: Cambridge, 1990.

Scheme 3. Photolysis Products of **1A** in Frozen Acetonitrile

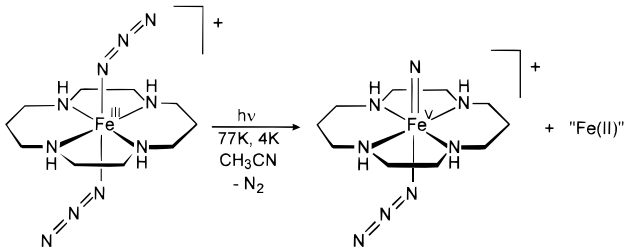

(iii) its low-spin Fe^{IV} (d^4) form in both dinuclear species containing the $[Fe^{IV}(\mu\text{-}N)Fe^{III}]^{4+}$ core with localized valencies ($S_t = {}^3/_2$ and $S_t = {}^1/_2$), and finally, (iv) the Fe^{V} ion in the low-temperature intermediate appear to be linearly correlated with the formal oxidation states of the iron ions. This is shown in Figure 14.

Theoretically, the Mössbauer isomer shift is a linear function of the charge density $|\Psi(0)|^2_A$ at the ^{57}Fe-absorber nucleus,[62] eq 6

$$\delta = -\alpha\{|\Psi(0)|^2_A - C\} \qquad (6)$$

where α accounts for general electronic and nuclear properties and C is a calibration constant depending on the isomer shift reference scale. The charge density $|\Psi(0)|^2_A$ at the nucleus is primarily determined by the s-electron density at ($r = 0$) which is sensitively affected by chemical bonds due to (i) direct alteration of the s population or (ii) indirect shielding of the nuclear potential by changes in the d population. Owing to the negative sign in eq 6, direct increasing of the s population decreases δ, whereas increasing the d population increases δ and vice versa. Approximately linear correlations of isomer shifts with formal oxidation states can be expected if the covalent variations in both s and d orbitals are small or practically linear. This behavior can be expected for the complexes assembled in Figure 14. In the whole series the iron ions are octahedrally coordinated with relatively "rigid" equatorial ligands from a macrocycle and smooth variations in the axial ligation. The complexes with Fe^{II}, Fe^{III}, and Fe^{IV} are clearly six-coordinate, and from the perfect match of the isomer shift correlation one can infer that the Fe^{V}═N intermediate is also six-coordinate. Schematically, the axial coordination in the series can be described as N_3-Fe-N_3 for Fe^{II} and Fe^{III}, N_3-Fe═N for Fe^{IV}, and N_3-Fe═N for Fe^{V}. Important for the consistency of the correlation diagram is also the fact that the formal electronic configuration of all complexes is $3d(t_{2g})^n(e_g)^0$.

Isomer shifts of highly oxidized compounds have been related to oxidation states before[62−65] partly based on the basis of theoretical charge densities derived from molecular orbital calculations.[64] The highest oxidation state considered in such a correlation was that of Fe^{VI} in ferrates,[64] which has the lowest isomer shift of all compounds measured, $\delta = -0.91$ mm s^{-1}.[66] To our knowledge the only other example of Mössbauer spectroscopically characterized octahedral iron complex with

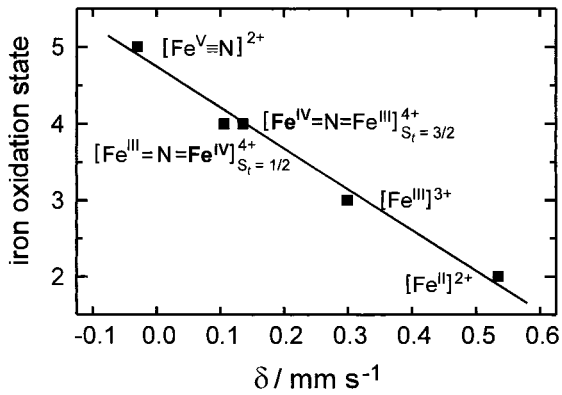

Figure 14. Plot of the isomer shift, δ, of complexes vs the formal oxidation state of the respective iron ion. Complexes from left to right: $[Fe^{V}{=}N]^{2+}$: *trans*-$[N{=}Fe^{V}(cyclam)(N_3)]^+$ or *trans*-$[N{=}Fe^{V}$-(cyclam)$]^{2+}$, $[Fe^{III}(\mu\text{-}N)Fe^{IV}]^{4+}$ ($S_t = {}^1/_2$): Fe^{IV} in the solution photolysis product of **1a**, $[Fe^{IV}(\mu\text{-}N)Fe^{III}]^{4+}$ ($S_t = {}^3/_2$): Fe^{IV} in the solution photolysis product of **2**, $[Fe^{III}]^{3+}$: low-spin Fe^{III} in **1a**, $[Fe^{II}]^{2+}$: low-spin Fe^{II} in one-electron reduced **1a**.

unambiguous Fe^{V} character is $La_2Li[FeO_6]$.[65,67] In this highly covalent compound which possesses also a $3d^3$ high-spin ($S = {}^3/_2$) configuration the isomer shift is -0.41 mm s^{-1}.[67] This low value for the oxygen-coordinate Fe^{V} in comparison with $\delta = -0.04$ mm s^{-1} for the Fe^{V}═N intermediate is qualitatively consistent with the stronger π-interaction of six strong oxygen π-donor ligands in $La_2[FeO_6]$ in comparison with essentially only one nitrido π-donor ligand in our case. Increasing covalency (within comparable systems) leads to more negative isomer shifts due to increased "delocalization" of iron 3d charge into the chemical bonds as well as due to directly increased iron s population, as the result of enhanced 3s-/4s-contributions to low-lying bonding MO's with ligand orbitals.[62] In this sense the coordination of Fe^{V} with six oxygen-donor ligands is more covalent than the coordination in the Fe^{V}═N intermediate with one π-donor and five σ-donor ligands. This suggests that the d_{xz},d_{yz} orbitals in the nitrido intermediate which are antibonding with respect to the axial ligand are only moderately destabilized by interaction with nitrogen p_x,p_y orbitals, which is in accord with the observed $S = {}^3/_2$ high-spin state due to $(d_{xy})^1(d_{xz})^1(d_{yz})^1$ configuration. The same conclusion was earlier drawn from resonance Raman data for a corresponding (porphyrin)Fe^{V}═N nitrido species.[17] It is further substantiated by the low zero-field splitting of the $S = {}^3/_2$ state which is in the usual range for $3d^3$ complexes, as it was observed, for instance, for many octahedral Cr^{3+} compounds.[68,69]

The large, negative quadrupole splitting of Fe^{V}═N as well as the high anisotropy of the hyperfine coupling tensor $\bar{\mathbf{A}}$ cannot be explained straightforwardly in a simple valence bond picture. According to the formally half-filled t_{2g} shell, the valence-contribution to the efg[62] should be zero. A similar situation is encountered in dimeric $Fe^{3+}-O-Fe^{3+}$ units which also show large quadrupole splittings of up to 2.45 mm s^{-1},[45,70,71] despite the "spherical" half-filled 3d valence shell of high-spin Fe^{3+}. There, the corresponding large efg's were attributed to non-spherical distributions of the charge of the ligand sphere and to covalency of the valence electron configuration of Fe^{3+} with a

(62) Gütlich, P.; Link, R.; Trautwein, A. *Mössbauer Spectroscopy and Transition Metal Chemistry*; Springer-Verlag: Berlin, Heidelberg, New York, 1978.
(63) Greenwood, N. N.; Gibb, T. C. *Mössbauer Spectroscopy*; Chapman and Hall Ltd.: London, 1971.
(64) Guenzburger, D.; Esquivel, D. M. S.; Danon, J. *Phys. Rev. B* **1978**, *18*, 4561.
(65) Russo, U.; Long, G. J. Mössbauer Spectroscopic Studies of the High oxidation States of Iron. In *Mössbauer Spectroscopy Applied to Inorganic Chemistry*; Russo, U., Long, G. J., Eds.; Plenum Press: New York, London, 1989; Vol. 3, p 289.
(66) Wertheim, G. K.; Herber, R. H. *J. Chem. Phys.* **1962**, *36*, 2497.
(67) Demazeau, G.; Buffat, B.; Pouchard, M.; Hagenmüller, P. *Z. Anorg. Allg. Chem.* **1982**, *491*, 60.
(68) Pedersen, E.; Toftlund, H. *Inorg. Chem.* **1974**, *13*, 1603.
(69) Singer, L. S. *J. Chem. Phys.* **1955**, *23*, 379.
(70) Atkin, C. L.; Thelander, L.; Reichard, P.; Lang, G. *J. Biol. Chem.* **1973**, *248*, 7464.
(71) Lynch, J. B.; Juarez-Garcia, C.; Münck, E.; Que, L. *J. Biol. Chem.* **1989**, *264*, 8091.

short (1.79 Å) oxo bond.[45] In our case we adopt the same arguments for the Fe^{V}-nitrido group. However, we can specifically exclude again strong covalency of the antibonding d_{xz},d_{yz} orbitals as major origin of the efg, because population deficiency of these orbitals would yield a positive sign for V_{zz}, in contrast to the experimental observations.

Conclusion

We have shown in this investigation that low-spin *trans*-$[(cyclam)Fe^{III}(N_3)_2]^+$ (d^5 $S = {}^1/_2$) yields upon one-electron reduction a low-spin ferrous complex *trans*-$[(cyclam)Fe^{II}(N_3)_2]$ (d^6 $S = 0$), whereas the isomeric complex *cis*-$[(cyclam)Fe^{III}(N_3)_2]^+$ is high-spin (d^5 $S = {}^5/_2$) and affords upon one-electron reduction the corresponding high-spin ferrous form (d^6 $S = 2$).

Photolysis of **1a** and **2** in dry acetonitrile *liquid solution* with UV−visible light efficiently generates dinuclear species containing the $[Fe(\mu\text{-}N)Fe]^{4+}$ core in >80−90% yield. The reaction of **1a** produces a species with an $S_t = {}^1/_2$ ground state with two on the Mössbauer time scale nonequivalent iron ions which are assigned to oxidation states Fe^{III} and Fe^{IV}. Thus, this species is a mixed-valent class II complex with a *localized* excess electron. The proposed structure is $[\{trans\text{-}[(cyclam)Fe(N_3)]\}_2(\mu\text{-}N)]^{2+}$ where an intermediate-spin ferric ion ($S = {}^3/_2$) and a low-spin Fe^{IV} ion ($S = 1$) are intramolecularly antiferromagnetically coupled, giving rise to the observed $S_t = {}^1/_2$ ground state.

Photolysis of **2** in CH_3CN *liquid solution* produces a similar mixed valent, dinuclear μ-nitrido bridged species but with an $S_t = {}^3/_2$ ground state. Mössbauer spectroscopy clearly shows that the valencies are *localized* and comprise a high-spin ferric ($S = {}^5/_2$) and a low-spin Fe^{IV} ion ($S = 1$). Intramolecular antiferromagnetic coupling generates the observed $S_t = {}^3/_2$ ground state. For this species we propose the following structure as the most likely one: $[\{trans\text{-}[(cyclam)Fe^{IV}(N_3)]\}(\mu\text{-}N)\{cis\text{-}[(cyclam)Fe^{III}(N_3)]\}]^{2+}$.

Finally, photolysis of **1a** in *frozen* CH_3CN *solution* at 4 and 77 K generates a mononuclear species with an $S = {}^3/_2$ ground state and Mössbauer parameters which are indicative of an oxidation state $+V$ at the iron ion with an $(d_{xy})^1(d_{xz})^1(d_{yz})^1$ electron configuration. We propose that these spectral features are due to the nitridoiron(V) species *trans*-$[N{=}Fe^{V}(cyclam)(N_3)]^+$. In addition, we have shown that *photoreduction* via $Fe^{III}-N_3$ bond homolysis generates a five-coordinate *trans*-$[(cyclam)Fe^{II}(N_3)]^+$ species with an $S = 2$ ground state. These results are summarized in Scheme 3.

Experimental Section

Preparation of Complexes. The ligand 1,4,8,11-tetraazacyclotetradecane (cyclam)[72] and the complex *cis*-$[(cyclam)Fe^{III}Cl_2]Cl$[23] were prepared according to published procedures.

^{57}Fe-enriched species were prepared as follows. Metallic ^{57}Fe (98%) (34.4 mg) and ^{56}Fe (foil) (59.9 mg) were dissolved in concentrated aqueous HCl (20 mL) with heating. $^{57/56}FeCl_3$ was obtained by complete evaporation of the acid under reduced pressure (rotary evaporation). The residue was dissolved in CH_3OH (10 mL). To this solution the ligand cyclam (0.49 g, 2.44 mmol) was added. After the mixture was heated to reflux for 60 min, a clear yellow solution was obtained. To the cooled solution 30% aqueous HCl was added dropwise, whereupon a microcrystalline precipitate of *cis*-[(cyclam) $^{57/56}Fe^{III}Cl_2]Cl$ formed which was collected by filtration. Yield: 0.59 g (94%). Electrospray ionization mass spectrometry (ESI) confirmed the isotopic labeling with 35% ^{57}Fe.

Caution. Although we have not encountered any problems it should be noted that perchlorate salts are potentially explosive. Small quantities should be prepared only and handled with the appropriate care.

(72) Barefield, K. E.; Wagner, F. *Inorg. Synth.* **1976**, *16*, 220.

***trans*-[(cyclam)$Fe^{III}(N_3)_2$]X (X = ClO_4 (1a), PF_6 (1b)).** To a hot (~50 °C) $HClO_4$ acidified solution of NaN_3 (2.0 g, 30.8 mmol) (pH ≈ 5) in a CH_3OH/H_2O mixture (50 mL, 10:1) was added *cis*-[(cyclam)-$Fe^{III}Cl_2]Cl$ (0.50 g, 1.38 mmol), whereupon a deep red solution was obtained. (**Caution**: effervescence of HN_3). The solution was stirred at 50 °C for 45 min and filtered. Addition of a saturated solution of $NaClO_4$ in CH_3OH (10 mL) initiated the precipitation of yellow-brown needle-shaped crystals of **1a**. Yield: 0.50 g (83%). The same reaction in a CH_3CN/H_2O mixture (1:1) which was acidified with HPF_6 afforded at 4 °C prismatic single crystals suitable for X-ray crystallography of **1b**. Anal. Calcd for $C_{10}H_{24}N_{10}FeClO_4$ (**1a**): C, 27.31; H, 5.50; N, 31.86. Found: C, 27.47; H, 5.47; N, 31.62.

***cis*-[(cyclam)$Fe^{III}(N_3)_2$](ClO_4) (2).** *cis*-$[(cyclam)Fe^{III}Cl_2]Cl$ (0.34 g, 0.94 mmol) was added to a solution of NaN_3 (1.0 g 15.4 mmol) in CH_3OH (80 mL) at −18 °C which was carefully acidified with perchloric acid (pH ≈ 5). The cooled red solution was stirred for 30 min. A red microcrystalline precipitate of **2** slowly formed at −18 °C which was collected by filtration, washed with cold CH_3OH and diethyl ether, and air-dried. Yield: 0.38 g (91%). Single crystals of **2** suitable for X-ray crystallography were grown from a saturated CH_3OH solution of **2** at −25 °C after addition of $NaClO_4$. Anal. Calcd for $C_{10}H_{24}N_{10}$-$FeClO_4$: C, 27.31; H, 5.50; N, 31.86. Found: C, 27.45; H, 5.69; N, 31.81.

Physical Measurements. Infrared spectra (400−4000 cm^{-1}) of solid samples were recorded on a Perkin-Elmer 2000 FT-IR/FT-NIR spectrometer as KBr disks. Cyclic voltammetric and Coulometric measurements were performed on EG & G equipment (potentiostat/galvanostat model 273A) on acetonitrile solutions of samples containing 0.10 M $[N(n\text{-}but)_4]PF_6$ as supporting electrolyte. UV−vis spectra of solutions were measured on a Perkin-Elmer Lambda 19 spectrophotometer in the range 200−1600 nm. Temperature-dependent magnetic susceptibilities of powdered samples were measured by using a SQUID magnetometer (Quantum Design) at 1.0 T (2.0−300 K). Corrections for underlying diamagnetism were made by using tabulated Pascal constants. X-band EPR spectra were recorded on a Bruker ESP 300E spectrometer equipped with a helium flow cryostat (Oxford Instruments ESR 910). Mössbauer data were recorded on an alternating constant-acceleration spectrometer. The minimum experimental line width was 0.24 mm s^{-1} (full width at half-height). The sample temperature was maintained constant either in an Oxford Instruments Variox or an Oxford Instruments Mössbauer-Spectromag 2000 cryostat. The latter is a split-pair superconducting magnet system for applied fields up to 8 T where the temperatures of the sample can be varied in the range 1.5−250 K. The field at the sample is oriented perpendicular to the γ-beam. The ^{57}Co/Rh source (1.8 GBq) was positioned at room temperature inside the gap of the magnet system at a zero-field position. Isomer shifts are quoted relative to iron metal at 300 K.

Low-temperature EPR, magnetic Mössbauer spectra, and magnetization measurements were analyzed on the basis of a spin-Hamiltonian description of the electronic ground-state spin multiplet

$$H_e = D[S_z^2 - S(S+1)/3 + (E/D)(S_x^2 - S_y^2)] + \mu_B \mathbf{B}\cdot\bar{g}\mathbf{S} \quad (7)$$

where $S = {}^5/_2$, $S = {}^3/_2$ or $S = {}^1/_2$ is the spin of the corresponding system and D and E/D are the axial and rhombic zero-field parameters for $S > {}^1/_2$. For the simulation of the Mössbauer spectra we have taken into account additionally the hyperfine Hamiltonian

$$H_{hf} = \mathbf{S}\cdot\bar{\mathbf{A}}\cdot\mathbf{I} - g_N\beta_N\mathbf{B}\cdot\mathbf{I} + H_Q \quad (8)$$

where <**S**> is the electronic spin expectation value, $\bar{\mathbf{A}}$ is the hyperfine coupling tensor, **I** is the nuclear spin and H_Q is the usual nuclear quadrupole Hamiltonian.[62,73] Spin-Hamiltonian simulations of EPR spectra were performed with a program which was developed from the $S = {}^5/_2$ routines of Gaffney and Silverstone[74] and which specifically makes use of the resonance-search procedure described therein. The

(73) Trautwein, A. X.; Bill, E.; Bominaar, E. L.; Winkler, H. *Struct. Bonding* **1991**, *78*, 1.

(74) Gaffney, B. J.; Silverstone, H. J. Simulation of the EMR Spectra of High-Spin Iron in Proteins. In *Biological Magnetic Resonance*; Berliner, L. J., Reuben, J., Eds.; Plenum Press: New York, London, 1993; Vol. 13.

EPR and Mössbauer spectra of the dimeric photolysis products of complexes **1a** and **2** were analyzed with the assumption of strong exchange coupling of the local spins S_i ($|J/D_i| \gg 1$). In eqs 7, 8, then, the total spin of the respective dimer ground state was inserted, and in eq 8 effective $\bar{\mathbf{A}}$ tensors, $\bar{\mathbf{A}}^{\mathrm{eff}}$, were used instead of the intrinsic values for the local iron spins. From an application of the Wigner−Eckart theorem the following relations of effective and intrinsic $\bar{\mathbf{A}}$ tensor components are derived:[75]

$$\text{(a)}\quad S_1 = 1(\mathrm{Fe^{IV}}),\quad S_2 = {}^5/_2(\mathrm{Fe^{III}}),\quad S_t = {}^3/_2$$

$$\bar{\mathbf{A}}(\mathrm{Fe^{IV}}) = -{}^5/_2\,\bar{\mathbf{A}}^{\mathrm{eff}}(\mathrm{Fe^{IV}}) \tag{9a}$$

$$\bar{\mathbf{A}}(\mathrm{Fe^{III}}) = +{}^5/_7\,\bar{\mathbf{A}}^{\mathrm{eff}}(\mathrm{Fe^{III}}) \tag{9b}$$

$$\text{(b)}\quad S_1 = 1(\mathrm{Fe^{IV}}),\quad S_2 = {}^3/_2(\mathrm{Fe^{III}}),\quad S_t = {}^1/_2$$

$$\bar{\mathbf{A}}(\mathrm{Fe^{IV}}) = -{}^3/_2\,\bar{\mathbf{A}}^{\mathrm{eff}}(\mathrm{Fe^{IV}}) \tag{10a}$$

$$\bar{\mathbf{A}}(\mathrm{Fe^{III}}) = +{}^3/_5\,\bar{\mathbf{A}}^{\mathrm{eff}}(\mathrm{Fe^{III}}) \tag{10b}$$

Photolysis Experiments. Photolysis reactions at −35 and 20 °C were carried out in variable-temperature quartz cells through which a stream of Ar gas was passed. A Hg immersion lamp (Osram, HPK 125) produced the UV-visible light used for irradiation or, alternatively, an Osram HBO 200 light source for the experiments in frozen solutions.

Photolyses of EPR and Mössbauer samples in frozen solution were first performed in situ at 4.2 K in the respective spectrometer cryostats (method I). For the EPR experiments the light of a Hg lamp (OSRAM, HBO200) was collimated and focused on a flexible quartz-fiber light guide and passed through the illumination grid of an EPR rectangular TE102 cavity (Bruker, ER4102) into a helium flow cryostat (Oxford Instruments ESR910) with quartz assembly. The ferric starting complex (1.75 mM in acetonitrile, 35% enriched in ^{57}Fe) was in a 4-mm standard EPR tube which was cooled during illumination with a high flow of liquid helium (∼1.5 L/hr). It was rotated stepwise by 90°. For the corresponding Mössbauer preparations the light of the Hg lamp was passed into a 4-mm quartz-rod that reached ∼1 m into the variable-temperature insert of an Mössbauer cryostat (Oxford Instruments, Variox or Spectromag 2000) with horizontal γ-beam. The flat Mössbauer absorber was a thin layer (1 mm) of frozen solution on a 0.5-mm Delrin support which was tilted against the γ-beam by about 70° (out of the plane-normal) and by about 20° against the light coming from the top. The sample holder had openings for efficient absorber cooling, and the cryostat insert was kept at about 800 hPa of helium exchange gas. During illumination (10 min to 2 h) the flow of liquid helium coolant through the heat exchanger was kept at about 1 L/hr. We estimate that the sample temperature did not exceed 15 K.

After initial measurements had shown that the photolysis products are stable up to 120 K another preparation protocol was applied for photolyses at 77 K, which started with powders of finely ground, frozen solutions under liquid nitrogen (LN_2) (**method II**). The ferric starting material (1.75 mM in acetonitrile, 35% enriched with ^{57}Fe) was slowly pipetted into a quartz cup filled with LN_2. The frozen drops were carefully milled in LN_2 by an ordinary magnetic stirrer which was placed under a Styrofoam vessel with LN_2 which prevented excessive boil-off from the quartz cup. These manipulations were performed in a polyethylene glovebag under a dry N_2 atmosphere. When a fine powder was obtained, the LN_2 bath with stirrer and quartz cup was transferred to a laboratory photolysis reactor (Rayonet Model RPR-100, equipped with 16 tubes for light in the range 185−419 nm). After illumination for 20−90 min with permanent stirring of the dispersed sample in LN_2 the quartz cup was taken back to an open LN_2 bath outsite the reactor where the sample powder was transferred with spatula and Teflon plungers to a Mössbauer cup (made of Delrin, ∅ 10 mm, height 9 mm) and a short (60 mm long, ∅ 4 mm) EPR tube. From test measurements with a small Pt-100 sensor we estimate that the sample temperature during transfer never exceeded 77 K for more than a few seconds and did not rise above 120 K.

Table 9. Crystallographic Data for Complexes **1b** and **2**

	1b	**2**
formula	$C_{10}H_{24}F_6FeN_{10}P$	$C_{10}H_{24}N_{10}FeClO_4$
formula wt (g·mol^{-1})	485.2	439.7
color and habit	orange/octahedron	red/octahedron
crystal system	monoclinic	monoclinic
space group	$P2_1/n$	$P2_1/c$
a, Å	7.858(1)	13.641(2)
b, Å	13.323(2)	8.851(1)
c, Å	9.335(1)	15.266(3)
β, deg	102.95(1)	99.53(1)
V, Å^3	952.4(2)	1817.7(1)
Z	2	4
T, K	293(2)	100(2)
d_{calcd}, g·cm^{-3}	1.692	1.607
radiation, (λ, Å)	0.71073	0.71073
μ, mm^{-1}	0.952	1.018
R1[a]	0.033	0.040
wR2[b]	0.086	0.085

[a] $R1 = \sum||F_o| - ||F_c||/\sum|F_o|$. [b] $\mathrm{wR2} = [\sum[w(F_o^2 - F_c^2)^2]/\sum[w(F_o)^2]]^{1/2}$.

X-ray Crystallography. A yellow-brown crystal of **1b** and a red crystal of **2** were sealed in glass capillaries. Graphite monochromated Mo Kα radiation (λ = 0.71073 Å) was used throughout. Crystallographic data are listed in Table 9. Intensity data were collected on an Enraf-Nonius CAD4 diffractometer using the $\omega-2\theta$ scan technique for **1b** at 293(2) K and those of **2** on a Siemens SMART CCD-detector system equipped with a cryogenic nitrogen cold stream at 100(2) K. Data collection for **2** was performed by a hemisphere run taking frames at 0.30° in ω. The data were corrected for Lorentz and polarization effects. A semiempirical absorption correction using the program SADABS[76] was performed for **2**, whereas for **1b** no absorption correction was carried out. The Siemens ShelXTL[77] software package was used for solution, refinement, and artwork of the structures. Both structures were solved and refined by direct methods and difference Fourier techniques performed on DEC Alpha workstations. Neutral atom scattering factors were used.[78] All non-hydrogen atoms were refined anisotropically. All hydrogen atoms were placed at calculated positions and refined as riding atoms with isotropic displacement parameters.

Acknowledgment. We thank the Fonds der Chemischen Industrie for financial support. We thank a reviewer for insightful comments with regard to the electronic structure of the room-temperature photolysis product of **1a**.

Supporting Information Available: Tables of crystallographic and structure refinement data, atom coordinates, bond lengths and angles, anisotropic thermal parameters, and calculated positional parameters of H atoms for complexes **1b**, **2** (PDF) and an X-ray crystallographic file in CIF format. This material is available free of charge via the Internet at http://pubs.acs.org.

JA983454T

(75) (a)Scaringe, P. R.; Derek, J. H.; Hatfield, W. E. *Mol. Phys.* **1978**, *35*, 701. (b) Bencini, A.; Gatteschi, D. *EPR of Exchange Coupled Systems*; Springer-Verlag: Berlin, 1990.

(76) Sheldrick, G. M. (Universität Göttingen) 1994.

(77) Siemens Industrial Automation, Inc. 1994.

(78) International Tables for X-ray Crystallography, Kynoch Press: Birmingham, England.